Downward Wave Reflection as a Mechanism for the Stratosphere–Troposphere Response to the 11-Yr Solar Cycle

HUA LU

British Antarctic Survey, High Cross, Cambridge, United Kingdom

ADAM A. SCAIFE

Met Office Hadley Centre, Exeter, United Kingdom

GARETH J. MARSHALL AND JOHN TURNER

British Antarctic Survey, High Cross, Cambridge, United Kingdom

LESLEY J. GRAY

NCAS-Climate, Department of Atmospheric Physics, Clarendon Laboratory,
Oxford University, Oxford, United Kingdom

ABSTRACT

The effects of solar activity on the stratospheric waveguides and downward reflection of planetary waves during NH early to midwinter are examined. Under high solar (HS) conditions, enhanced westerly winds in the subtropical upper stratosphere and the associated changes in the zonal wind curvature led to an altered waveguide geometry across the winter period in the upper stratosphere. In particular, the condition for barotropic instability was more frequently met at 1 hPa near the polar-night jet centered at about 55°N. In early winter, the corresponding change in wave forcing was characterized by a vertical dipole pattern of the Eliassen–Palm (E–P) flux divergent anomalies in the high-latitude upper stratosphere accompanied by poleward E–P flux anomalies. These wave forcing anomalies corresponded with negative vertical shear of zonal mean winds and the formation of a vertical reflecting surface. Enhanced downward E–P flux anomalies appeared below the negative shear zone; they coincided with more frequent occurrence of negative daily heat fluxes and were associated with eastward acceleration and downward group velocity. These downward-reflected wave anomalies had a detectable effect on the vertical structure of planetary waves during November–January. The associated changes in tropospheric geopotential height contributed to a more positive phase of the North Atlantic Oscillation in January and February. These results suggest that downward reflection may act as a "top down" pathway by which the effects of solar ultraviolet (UV) radiation in the upper stratosphere can be transmitted to the troposphere.

1. Introduction

Ozone absorption of solar radiation in the ultraviolet (UV) band is known to affect upper-atmospheric chemistry and temperature, and thus its circulation via photochemical, radiative, and dynamical interactions (Brasseur and Solomon 2005). The enhanced UV forcing during high solar (HS) activity years leads to a 2%–4% increase of annual mean stratospheric ozone and an approximate 1-K increase of annual mean temperature in the equatorial upper stratosphere and lower mesosphere (e.g., Haigh 1994; Scaife et al. 2000; Hood 2004; Frame and Gray 2010; Chiodo et al. 2012; Hood and Soukharev 2012; Mitchell et al. 2014; Hood et al. 2015). While these upper-atmospheric ozone and temperature anomalies are generally well understood, the extent to which they can be transferred downward to affect the lower stratosphere and the troposphere remains a subject of scientific investigation (Gray et al. 2010).

Studies show that a regional circulation pattern in the Northern Hemisphere (NH) winter that resembles the

Corresponding author e-mail: Hua Lu, hlu@bas.ac.uk; hlu@bas.ac.uk; gjma@bas.ac.uk; jtu@bas.ac.uk; adam.scaife@metoffice.gov.uk; gray@atm.ox.ac.uk

positive phase of the North Atlantic Oscillation (NAO) occur during HS winters (e.g., Ruzmaikin and Feynman 2002; Kodera 2002; Woollings et al. 2010b; Lockwood et al. 2010; Ineson et al. 2011; Gray et al. 2013, 2016). A number of different mechanisms have been proposed to explain this solar–NAO connection. A "top down" mechanism, first proposed by Hines (1974) and later developed by Kodera (1995), is often invoked to account for the downward transfer of a solar UV signal from the upper stratosphere (e.g., Kodera and Kuroda 2002; Matthes et al. 2004, 2006; Ineson et al. 2011; Thiéblemont et al. 2015). This mechanism comprises two main pathways. Higher UV forcing in HS years leads to increased latitudinal temperature gradients and hence anomalously strong westerlies in the subtropical upper stratosphere/lower mesosphere in early winter. The presence of this subtropical wind anomaly influences the propagation of midlatitude planetary-scale waves, resulting in a positive feedback between planetary waves and the polar vortex. As the winter progresses, the upper-level subtropical zonal mean wind anomaly moves poleward and extends downward into the lower stratosphere (Kodera and Kuroda 2002), where it perturbs the tropospheric circulation (Kidston et al. 2015). Associated with this is a modulation of the strength of the stratospheric meridional overturning circulation, with a weakened circulation and warmer tropical lower stratosphere in HS years due to weaker wave forcing in the extratropical stratosphere. An increase in lower tropical stratospheric temperature is also associated with a poleward expansion of the Hadley Cell, and the modulated lower stratospheric temperature gradients can influence synoptic wave propagation and/or breaking, resulting in a poleward shift of the tropospheric eddy-driven jet and a positive NAO in HS years (Haigh et al. 2005; Simpson et al. 2009).

Observational studies of sea level pressure during December–February have also shown that the overall maximum amplitude of the NAO-like solar response is found to lag the peak in solar variability by one-quarter cycle, with a maximum positive NAO-like response of 2–4 yr following solar maxima (Gray et al. 2013). An additional mechanism has been proposed to explain this lagged response, in which the sea surface temperature (SST) anomaly associated with the NAO forcing persists beneath the ocean mixed layer during the intervening summertime and reemerges the following winter, thus providing a positive feedback to the NAO forcing (Scaife et al. 2013; Andrews et al. 2015).

The aforementioned mechanisms and pathways have been evaluated by a wide range of modeling studies (e.g., Balachandran et al. 1999; Tourpali et al. 2003; Matthes et al. 2004; 2006; Rozanov et al. 2004; Schmidt

et al. 2010; Ineson et al. 2011; Cnossen et al. 2011; Chiodo et al. 2012; Andrews et al. 2015; Thiéblemont et al. 2015). Uncertainty over the robustness of the troposphere signal and the mechanisms responsible remains resulting from a large scatter of atmospheric responses among model simulations (Gray et al. 2010). A recent study based on the ensemble model simulations from phase 5 of the Coupled Model Intercomparison Project (CMIP5) showed that the top-down mechanism can only be reproduced by a few models, even with enhanced model resolution, interactive chemistry, and/or air–sea interaction (Mitchell et al. 2015). In addition, the classic polar route proposed by Kodera and Kuroda (2002) involves the downward transfer of zonal wind anomalies to the lower stratosphere, associated with the occurrence or absence of stratospheric warming events, and these are most prevalent during January–February. However, there is some evidence of a solar cycle signal in the troposphere that appears in early winter; for example, in Fig. 3 of Gray et al. (2004) and Fig. 9 of Mitchell et al. (2014), there is a statistically significant signal in the tropospheric zonal winds as early as December without the presence of an appropriate wind anomaly in the lower stratosphere.

A mechanism that is able to provide faster tropospheric response to upper-stratospheric perturbation is downward wave reflection. In particular, resonance occurs when the reflected planetary wave is well phased in relation to a wave near the surface. As such, a small perturbation in height could lead to a large response near the surface. Recent observational studies have demonstrated that a reflecting surface regularly forms in the high-latitude upper stratosphere during winter, causing downward reflection of planetary stationary waves into the troposphere (Harnik and Lindzen 2001; Perlwitz and Harnik 2003; Shaw et al. 2010). This downward reflection leads to a detectable effect on the amplitude, phase, and vertical structure of planetary waves, as well as tropospheric anomalies that resemble the positive phase of the NAO (Shaw and Perlwitz 2013). In contrast to the classic mechanism of Kodera and Kuroda (2002), the wave reflection mechanism does not require downward propagation of wind anomalies to the lower stratosphere. It has long been speculated that solar-UV-induced changes in the upper atmosphere can alter the reflection and/or absorption of planetary waves, whereby it is able to induce circulation changes in the troposphere (Hines 1974). Such an effect has yet to be properly quantified.

This paper aims to examine the solar cycle effect on downward wave reflection. We provide evidence to suggest that planetary wave reflection via changes of potential vorticity near the upper-stratospheric westerly
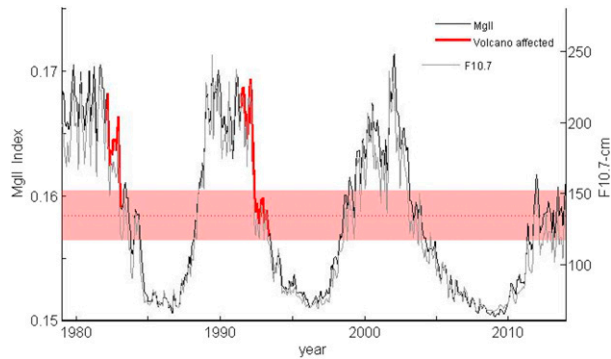
FIG. 1. Time series of monthly Mg II core-to-wing solar index (solid black line). Data above and below the red-shaded region (i.e., mean Mg II index ±0.002) denote HS and LS activity. Data within the red-shaded region and data that were contaminated by the major volcanic eruptions (i.e., the two red sections overlaid onto the black line) are excluded from the composite analysis. The commonly used F10.7 cm (10^{-22} W m^{-2} Hz^{-1}) is plotted for comparison (gray line).

jet could be an additional mechanism for the downward transfer of solar UV-induced anomalies to the troposphere.

2. Data and methods

The study makes use of daily data from the European Centre for Medium-Range Weather Forecasts (ECMWF) interim reanalysis (ERA-Interim) for 1979–2013 with 37 levels up to 1 hPa (Dee et al. 2011). This dataset is chosen because it has a good representation for the circulation and wave forcing in the upper stratosphere (Dee and Uppala 2009; Lu et al. 2015), where the influence of solar UV variability is greatest (Hood 2004; Kodera and Kuroda 2002). Note that the model employed for ERA-Interim does not include solar cycle variability in either the irradiance or ozone fields, so any signals are due to the assimilated observations.

The daily Mg II core-to-wing index for the 1979–2013 period (Viereck and Puga 1999) is used to represent solar UV variation. These data were developed using the Mg II core-to-wing ratio derived from the *Nimbus-7* Solar Backscatter UV (SBUV) radiometer on board several spaceborne instruments, including *UARS* and SBUV/2, and were calibrated based on the Mg II core-to-wing ratio from the Solar Stellar Irradiance Comparison Experiment (SOLSTICE) and the high-spectral-resolution Global Ozone Monitoring Experiment (GOME) instrument (de Toma et al. 1997). Monthly mean Mg II index (black line) is plotted on Fig. 1, in comparison with the commonly used solar flux (gray line) at 10.7 cm (F10.7 cm). Both solar indices are nearly in phase through the 11-yr solar cycle, except that the Mg II index has a smaller variation at the solar maximum.

Contamination of the solar signal by major ENSO events and volcanic eruptions was examined by excluding and including the winters affected by those events. We found that the results were not sensitive to inclusion of the major ENSO events, but, following Chiodo et al. (2014), we excluded three winters affected by major volcanic eruptions (Fig. 1) to avoid aliasing of volcanic signals. In addition, five solar neutral years (Fig. 1) were also excluded. Thus, the monthly and seasonal analyses were based on 12 high solar activity winters (1979/80, 1980/81, 1981/82, 1988/89, 1989/90, 1990/91, 1999/00, 2000/01, 2001/02, 2002/03, 2003/04, and 2011/12) and 16 low solar activity winters (1984/85, 1985/86, 1986/87, 1987/88, 1993/94, 1994/95, 1995/96, 1996/97, 1997/98, 2004/05, 2005/06, 2006/07, 2007/08, 2008/09, 2009/10, and 2010/11). Studies suggest that the 11-yr solar signal could be further modulated by the quasi-biennial oscillation (QBO) and geomagnetic activity (e.g., Labitzke 1987; Lu et al. 2007, 2009). However, these additional factors were not considered here because statistical significance may not be robustly obtained with any further subsampling, given the limited sample size.

Running composites using a centered 31-day running average window were performed for a range of diagnostic variables. The averages were used to reduce contamination from short-term internal variability, with the running window stepping forward in time on a daily interval. We found that qualitatively similar results were obtained by using an averaging window ranging from 31 to 45 days. Three-month-averaged Mg II indices for the months preceding the last day of the running average window were used to separate the data into HS and low solar (LS) conditions, depending on whether the averaged Mg II indices were greater or smaller than its seasonal mean plus or minus 0.002. As such, the solar signal obtained primarily indicates the atmospheric response to the lower-frequency (i.e., 11-yr and longer) solar irradiance variations rather than the short-term fluctuation associated with the approximate 27-day solar rotation. Also, the 3-month averaging of the Mg II index only builds a small lag into the analysis since our aim is to investigate the direct atmospheric response rather than the additional feedback from the ocean. For simplicity, the high and low solar irradiance composite groups are denoted hereafter as HS and LS, respectively.

a. The E–P flux divergence

Downward influence of radiative perturbations in the upper stratosphere arises through changes in planetary wave propagation, absorption, and/or reflection (Hines 1974; Shepherd and Shaw 2004). E–P fluxes and divergence diagnostics are employed to examine the 11-yr

solar cycle modulation of planetary wave activity (Andrews et al. 1987). The divergence is calculated by

$$\nabla \cdot \mathbf{F} = \frac{1}{a\cos\phi}[F^{(\phi)}\cos\phi]_\phi + F^{(z)}, \quad (1)$$

and the meridional and vertical fluxes are estimated by

$$F^{(\phi)} = \rho_0 a \cos\phi \left(\frac{\overline{v'\theta'}}{\theta_z}\overline{u}_z - \overline{v'u'}\right) \quad \text{and}$$

$$F^{(z)} = \rho_0 a \cos\phi \left\{\left[f - \frac{1}{a\cos\phi}(\overline{u}\cos\phi)_\phi\right]\frac{\overline{v'\theta'}}{\theta_z} - \overline{w'u'}\right\}, \quad (2)$$

where a is the mean radius of Earth; ϕ is latitude; f is the Coriolis parameter; θ is potential temperature; u, v, and w are zonal, meridional, and vertical velocities; z is the log-pressure height; the overbar denotes zonal average; subscripts denote derivatives; and primes denote departure from the zonal mean.

Stratospheric wave forcing is dominated by planetary waves, while tropospheric wave breaking is mainly associated with synoptic scale waves. The E–P fluxes and divergence diagnostics are therefore calculated separately for planetary waves (zonal wavenumbers 1–3). Also, transient waves tend to be generated near the reflecting surfaces, causing interference between stationary and traveling waves and thus transient fluctuations in the direction and magnitude of the waves (Shaw and Perlwitz 2013). To isolate changes in stationary planetary waves, 2–3-month averages are used to remove transient effects.

b. Measures of the stratospheric waveguide

Propagation of stationary planetary waves is primarily controlled by the ratio of the meridional gradient of the zonal mean potential vorticity (PV) gradient to the zonal mean westerly wind $\overline{u}$, with strong zonal wind and/or a small or negative PV gradient leading to wave reflection and/or absorption (Charney and Drazin 1961; Andrews et al. 1987). In spherical coordinates, quasigeostrophic zonal mean PV gradient takes the following form:

$$\overline{q}_\phi = 2\Omega\cos\phi - \underbrace{\left[\frac{(\overline{u}\cos\phi)_\phi}{a\cos\phi}\right]_\phi}_{\overline{q}_{\phi,m}} + \underbrace{\frac{af^2}{N^2}\left(\frac{\overline{u}_z}{H} - \overline{u}_{zz}\right)}_{\overline{q}_{\phi,z}}, \quad (3)$$

where Ω is Earth's angular velocity, H is the mean scale height ($=7\,\mathrm{km}$), and N is the buoyancy frequency, while other variables are defined previously in section 2a. Note that $\overline{q}_{\phi,m}$ and $\overline{q}_{\phi,z}$ denote the terms that represent the meridional and vertical components of $\overline{q}_\phi$. Wave reflection and/or absorption occur when $\overline{q}_\phi \leq 0$ (Harnik and Lindzen 2001). In the subtropical upper stratosphere and subtropical upper troposphere, where Rossby wave propagation is primarily horizontal toward the equator, intuitively one might expect that the condition reduces to $\overline{q}_{\phi,m} \leq 0$. In the high-latitude lower-to-middle stratosphere, where upward-propagating planetary waves dominate, we would then expect that wave breaking and/or reflection to occur when $\overline{q}_{\phi,z} \leq 0$. In addition, we note that wave reflection is indicated by little change or even enhanced westerlies near the reflecting surface with no gradual descent of zonal mean anomalies. Conversely, wave absorption leads to deceleration of the westerlies and is accompanied by downward descent of easterly anomalies. Following from Eq. (3), it was previously found that a suitable configuration for downward wave reflection in the high-latitude NH winter is a region with negative vertical wind shear ($\overline{u}_z < 0$) in the upper stratosphere, in addition to a stable polar vortex (Harnik and Lindzen 2001; Perlwitz and Harnik 2003, 2004; Shaw et al. 2010). Together with zonal mean wind anomalies, these conditions are used as the criteria to differentiate vertical coupling via a downward wave reflection from the downward descent of zonal-mean anomalies associated with wave absorption.

3. Results

a. Changes in circulation variables

Figure 2 shows the seasonal progression of climatological zonal-mean zonal wind and temperature and the associated solar composite differences (HS − LS) from November to March. The enduring feature of the difference plots throughout the winter is the persistent warm anomaly in HS compared to LS ($\sim$1.5–2K) in the equatorial upper stratosphere (0°–20°N and 1–3 hPa; Figs. 2f–j). This anomaly is consistent with the proposed mechanism for the influence of solar UV variability and agrees well with a study that examined the solar signal in nine different reanalysis datasets, including ERA-Interim (see Fig. 10 of Mitchell et al. 2014). As noted in earlier studies (e.g., Kodera and Kuroda 2002), there is an associated zonal wind anomaly in the subtropical upper stratosphere (Figs. 2k,l). This wind anomaly is confined to low latitudes during early winter (November–December), and, although there is some indication that it extends poleward and downward in January–February, the signal is not statistically significant. At high latitudes, there is some suggestion of a generally colder, stronger vortex in December–January in HS years, as expected from the classic polar
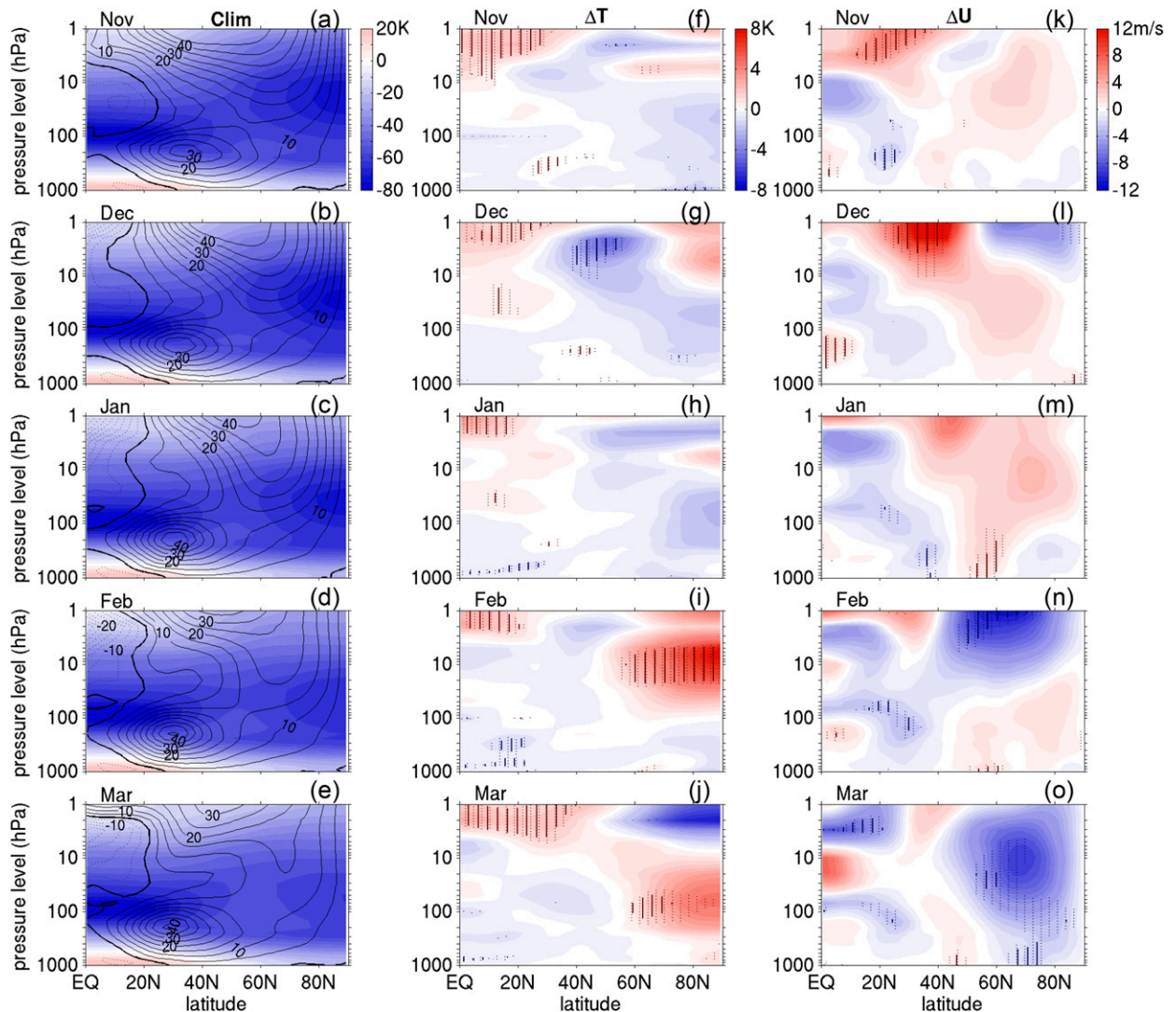
FIG. 2. (a)–(e) Seasonal march (November–March) of climatological zonal-mean temperature (shaded) and zonal wind (contours; m s^{-1}). Composite differences (HS − LS) for (f)–(j) temperature and (k)–(o) wind, where the vertical dotted and solid lines indicate the p value ≤ 0.1 and 0.05, calculated using a two-sided Student's t test.

mechanism for solar influence, but the signal shows no statistically significant response until February, by which time it is reversed in sign, with a warmer stratospheric vortex in HS years (and this anomaly persists at lower levels until March) (i.e., Figs. 2n,o). This switch in sign of the response is consistent with earlier studies (Gray et al. 2004) and supports the hypothesis that the solar cycle influence primarily affects the timing of stratospheric warming events, with earlier warmings under LS conditions and later warmings under HS conditions.

An important feature to note is the appearance of a statistically significant signal in the troposphere as early as January, when a dipole pattern with westerly

anomalies at 55°–60°N and easterly anomalies at 35°–40°N emerges (500–1000 hPa), implying a poleward shift of the tropospheric eddy-driven jet under HS. This dipole structure persists and evolves throughout the winter. The subtropical easterly anomaly around 20°–40°N is present throughout the winter and can be traced back as early as November. Toward the end of winter, the dipole anomaly of winds is found at higher latitudes, with a positive anomaly (e.g., in March) around 35°–50°N and negative anomaly poleward of 60°N.

The spatial distribution of the tropospheric zonal wind anomaly can be seen more clearly in Fig. 3, which shows January–February mean zonal winds at 200 hPa and sea level pressure and their corresponding solar signals. The
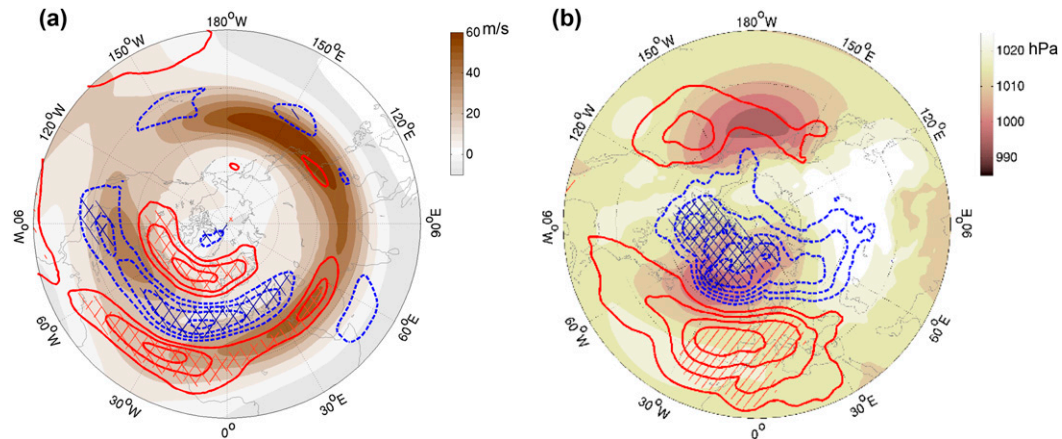
FIG. 3. Longitude–latitude (20°–90°N) cross section of January–February mean climatology (shaded) and solar cycle composite differences (HS − LS; contours) for (a) zonal mean wind at 200 hPa and (b) sea level pressure. The solid red contours are positive, and the dashed blue contours indicate negative for the differences. The contour interval is 1 m s^{-1} for the winds and 1 hPa for the pressure. The forward and backward hatches indicate the p value ≤ 0.1 and 0.05, respectively.

wind anomalies are marked by a poleward shift of the eddy-driven westerly jet under HS conditions compared with LS conditions, as well as an enhanced subtropical jet in the Atlantic sector. The combined effect of these wind anomalies is an enhanced separation between the eddy-driven jet and the subtropical jet, suggesting that a double-jet structure is more likely to occur over the Atlantic sector under HS, while a single, midlatitude westerly jet is more likely to be found under LS. The surface pressure anomalies are characterized by a strengthened pressure gradient between the high and midlatitudes in the North Atlantic region. Both the wind and pressure anomaly patterns indicate that the tropospheric response to the 11-yr solar cycle projects positively onto the NAO. However, the anomaly patterns differ

slightly from the classical NAO pattern because of their eastward extension (i.e., the signals are shifted more toward western Europe) and relatively weaker midlatitude response. This secondary effect resembles a negative east Atlantic (EA) pattern (Woollings et al. 2010a).

Figure 4 shows the climatology and solar composite differences of geopotential height at 850 hPa starting from 16 November (Fig. 4a), 1 December (Fig. 4b), and 16 December (Fig. 4c), each averaged over a period of 61 days. The solar signal starts to emerge from mid-November over the Arctic, where the effect is marked by negative height anomalies. The effect is followed by moderately significant (at the $p = 0.1$ level) positive height anomalies over the northeastern Atlantic around December. These height anomalies were found to be
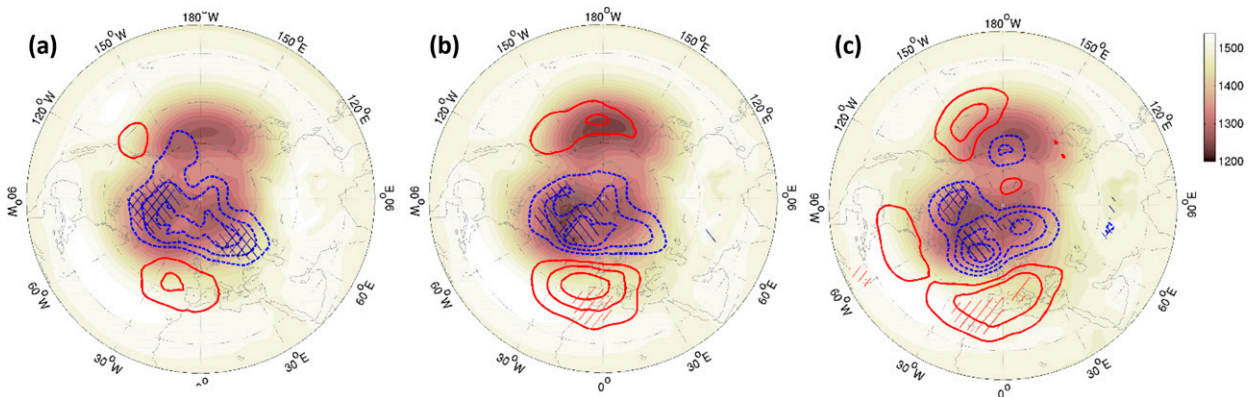
FIG. 4. Longitude–latitude (20°–90°N) cross section of 61-day averaged geopotential height climatology (shaded; m) and solar cycle composite differences (HS − LS; contours) with a starting date of (a) 16 Nov, (b) 1 Dec, and (c) 16 Dec at 850 hPa. The solid red contours are positive, and the dashed blue contours indicate negative for the differences. The contour interval is ±10 m, and the hatched regions indicate the differences achieved with a p value ≤ 0.1 and 0.05, respectively.
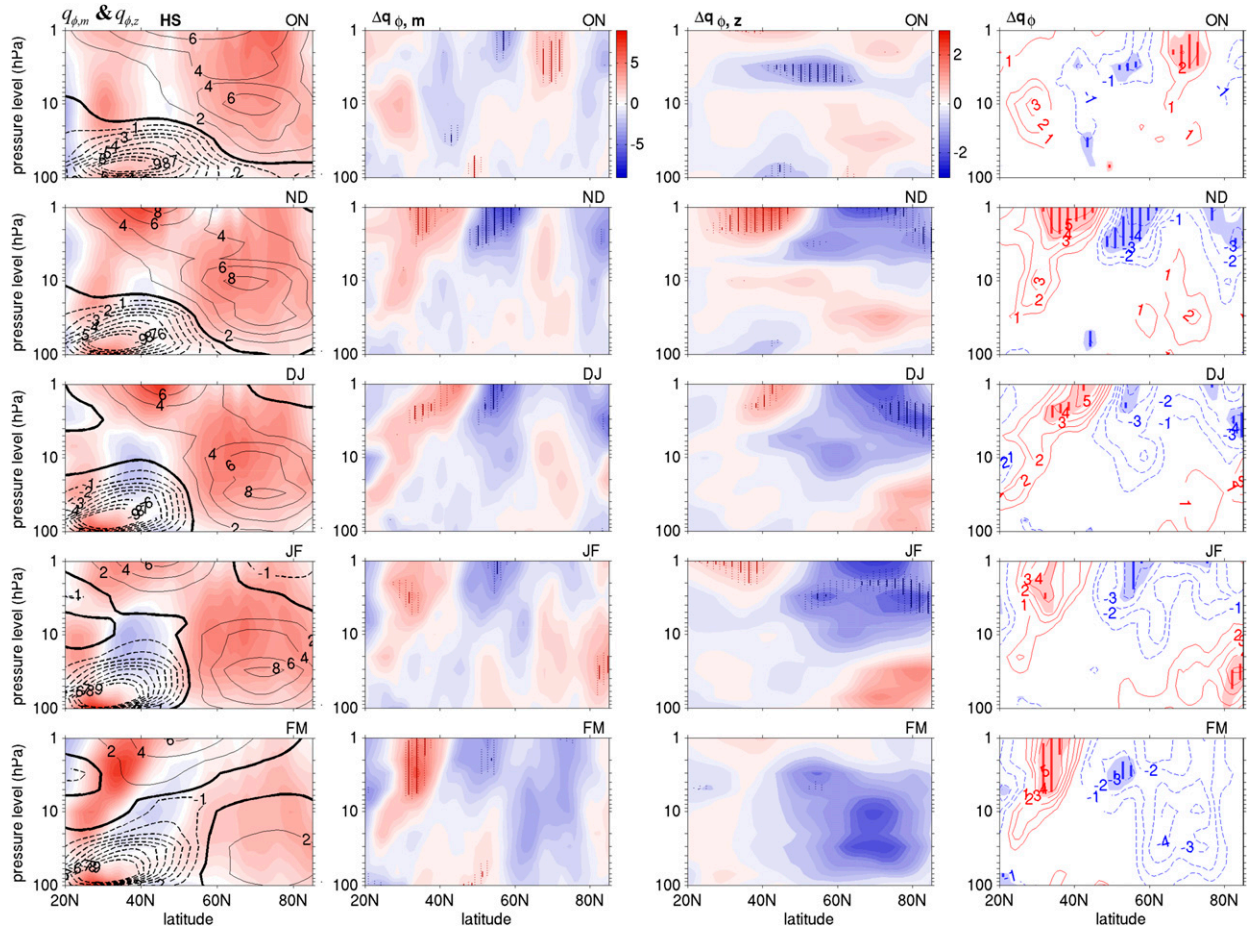
FIG. 5. (left) Seasonal march (2-month averages from ON to FM) of the horizontal (shaded) and vertical (contours) components of the PV gradient ($\times 10^5 \, s^{-1}$) under HS conditions (climatology + anomalies), all displayed in latitude–height cross sections of the stratosphere (20°–85°N and 100–1 hPa). (left center),(right center) Corresponding composite differences (HS − LS) for the horizontal and vertical components. (right) Composite differences (HS − LS) of the total meridional PV gradient, where red and blue contours indicate positive and negative anomalies. The vertical dotted and solid lines in (left center) and (right center) indicate the p value ≤ 0.1 and 0.05 for the differences. The regions that are shaded and heavily lined in (right) indicate the same statistical measures, all calculated using two-sided Student's t test.

most significant at and below the 850-hPa level and become increasingly noisier at levels above 850 hPa.

Figure 4 thus indicates that the tropospheric solar cycle signal starts as early as mid-November in the high-latitude lower troposphere, and the effect persists until mid-February. A positive NAO-like anomaly follows in January and February (Fig. 3). In the stratosphere, the polar vortex is stronger in early winter but weaker in late winter during HS years, consistent with a delay in sudden warming. We note that the classic mechanism built upon downward propagation of zonal mean anomalies explains neither the early winter tropospheric anomalies nor the late winter reversal of stratospheric response. The evidence provided so far instead suggests the existence of a faster, high-latitude route for solar influence. Indeed, previous studies have shown that downward

wave reflection from the high-latitude upper stratosphere leads to a positive NAO-like pattern in the extratropical troposphere, and the corresponding changes first emerge in the high-latitude lower troposphere (Shaw and Perlwitz 2013). In the remainder of the paper we provide the evidence that downward wave reflection acts as a faster, high-latitude pathway for downward transfer of solar UV perturbation.

b. Changes in the stratospheric waveguide

This section provides evidence of solar cycle–induced changes in stratospheric PV gradients, which are indicators of planetary wave propagation, absorption, and/or reflection.

Figure 5, left, shows the seasonal evolution of the meridional ($\overline{q}_{\phi,m}$; shaded) and vertical ($\overline{q}_{\phi,z}$; contours)

components of the PV gradient $\overline{q}_\phi$ at HS (note that absolute values rather than the anomalies are shown). The corresponding solar composite differences are shown in the center columns of Fig. 5, where regions with significant differences are indicated by vertical hatching. The composite difference of the total PV gradient $\overline{q}_\phi$ is also shown in Fig. 5, right. From October–November (ON) to February–March (FM), 2-month averages are used to better capture changes in the background conditions.

The stratospheric distribution of $\overline{q}_{\phi,m}$ during northern winter under HS (shaded values in Fig. 5, left) is marked by positive $\overline{q}_{\phi,m}$ in the high-latitude middle stratosphere and small and/or negative $\overline{q}_{\phi,m}$ in the region of 35°–45°N and 5–50 hPa. These features are also found under LS (not shown). In the upper stratosphere, $\overline{q}_{\phi,m}$ is generally positive in the subtropics and polar region, but it is close to zero at about 45°N and 1–2 hPa in October–November. The region with small $\overline{q}_{\phi,m}$ then moves slightly poleward as the winter progresses. Significant differences of $\overline{q}_{\phi,m}$ between HS and LS occur near this region, where the signal in $\overline{q}_{\phi,m}$ (Fig. 5, left center) is marked by a dipole pattern with positive anomalies at 20°–40°N and negative anomalies at 45°–60°N, both at 1–3 hPa. This dipole pattern of $\overline{q}_{\phi,m}$ anomalies is found throughout the entire winter season but is most significant during November–December.

The solar cycle signal in $\overline{q}_{\phi,z}$ (Fig. 5, right center) is also mostly found in the upper stratosphere, where the signal is broadly similar to that of $\overline{q}_{\phi,m}$ but shifted slightly poleward. The anomalies are marked by a dipole pattern, with positive anomalies at 25°–45°N and negative anomalies poleward of 55°N. The signal is most significant at approximately 2–5 hPa in the high latitudes and during November–February. These negative $\overline{q}_{\phi,z}$ anomalies result in negative anomalies of the total PV gradient $\overline{q}_\phi$ (Fig. 5, right) in the high-latitude upper stratosphere, where downward and equatorward expansion of the absolute negative $\overline{q}_{\phi,z}$ values are found under HS (see contours in Fig. 5, left).

Away from the polar region, the solar signal in the total PV gradient $\overline{q}_\phi$ is marked by positive anomalies at 20°–40°N and negative anomalies at 45°–60°N in the upper stratosphere. The pattern largely resembles the $\overline{q}_{\phi,m}$ anomalies, suggesting that the meridional component of the PV gradient plays a predominant role in this region. The anomalies are present throughout the winter months from November to March, but are strongest and most significant during November–December.

Previous studies suggest that the vertical component of the PV gradient $\overline{q}_{\phi,z}$, especially the vertical wind shear $\overline{u}_z$, plays an important role in causing downward wave reflection from the high-latitude upper stratosphere

(Perlwitz and Harnik 2003, 2004; Shaw et al. 2010). Figure 6 shows a further break down of $\overline{q}_{\phi,z}$ into the vertical wind shear and curvature and the corresponding solar cycle composite differences (HS − LS). The signal in the vertical shear is marked by negative anomalies in the high-latitude upper stratosphere and positive values in the subtropics, a pattern broadly similar to that in $\overline{q}_{\phi,z}$ (Fig. 5, right center). The effect is most significant during December–February and at 65°–85°N and 2–7 hPa. Thus, a solar cycle modulation of vertical PV gradient $\overline{q}_{\phi,z}$ at high latitudes is largely determined by the enhanced negative vertical shear there. The effect on vertical wind curvature is characterized by negative anomalies in the extratropical stratosphere. The signal in curvature sits just below the vertical shear anomalies, a configuration previously found to promote the formation of a reflecting surface for vertically propagating waves at high latitudes (Perlwitz and Harnik 2003, 2004; Shaw et al. 2010).

Three key regions in the upper stratosphere are selected to show the difference in terms of the temporal evolution of the absolute values of the PV gradients under HS and LS conditions based on 31-day running averages from 1 October to 31 March (Fig. 7). The horizontal PV gradients $\overline{q}_{\phi,m}$ at 35°–45°N and 55°–60°N in the upper stratosphere (1–3 hPa) are shown in Figs. 7a and 7b, respectively, representing the most significant changes near the upper-stratospheric westerlies. At 35°–45°N (Fig. 7a), $\overline{q}_{\phi,m}$ is generally larger under HS than LS, while the opposite holds at 55°–60°N (Fig. 7b). The temporal evolution of $\overline{q}_{\phi,m}$ in both regions is characterized by a double-peak structure in November–December and February–March, and the absolute values of the peaks are noticeably larger under HS than LS. Also, in both regions, $\overline{q}_{\phi,m}$ takes a longer time to reach its first peak (or trough) under HS and subsequently leads to a noticeable delay (~15 days) in its seasonal development. These results suggest that enhanced solar UV during solar maximum winters leads to enhanced meridional waveguides at 35°–45°N and reduced meridional waveguides at 55°–60°N. They indicate a sharpening of the PV gradient on the equatorward flank of the upper-stratospheric westerly jet, accompanied by enhanced PV mixing on its poleward flank. Such changes are accompanied by a prolonged development and greater seasonal variation of the waveguides in the midlatitude upper stratosphere. In particular, $\overline{q}_{\phi,m}$ at 55°–60°N becomes predominantly small, or even negative, under HS but remains largely positive under LS conditions. While waves tend to be refracted toward the region with larger values of $\overline{q}_\phi$, waves propagating toward a region of reduced PV gradients would also grow in amplitude as a result of
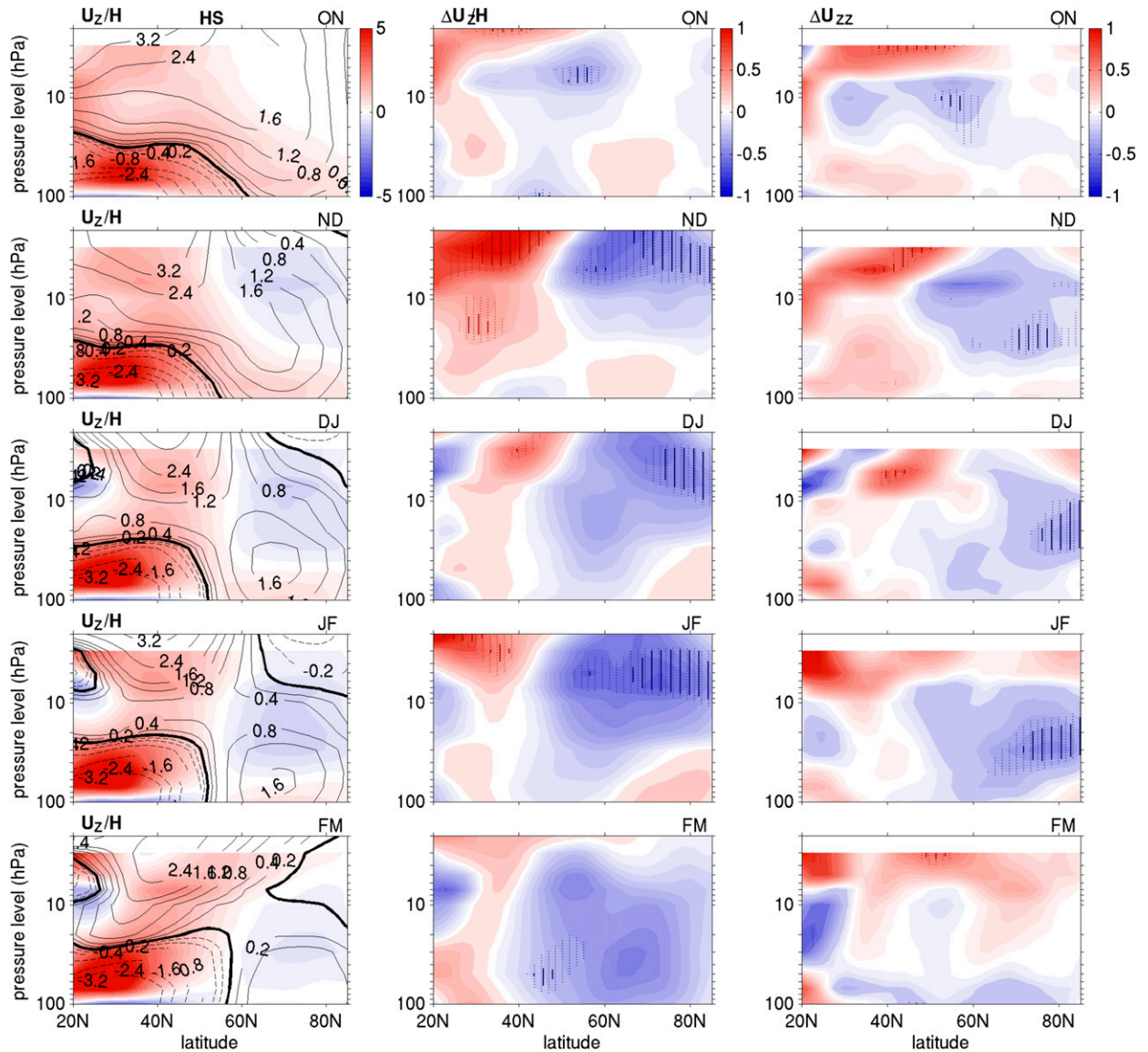
FIG. 6. (left) Seasonal march (2-month averages from ON to FM) of the height-scaled vertical wind shear ($\overline{u}_z/H$; $s^{-1}\,m^{-1}$; contours) and vertical curvature ($\overline{u}_{zz}$; $s^{-1}\,m^{-1}$; shaded) under HS conditions (climatology + anomalies). (center),(right) Corresponding solar composite differences (HS − LS), where the vertical dotted and solid lines indicate the p value ≤ 0.1 and 0.05, respectively, calculated using a two-sided Student's t test. Note that $\overline{u}_z/H$ and $\overline{u}_{zz}$ are scaled by a factor of 10^7 for clarity.

conservation of wave activity (James 1994). According to the Rayleigh–Kuo criterion, a change in the sign of $\overline{q}_{\phi,m}$ is a necessary condition for barotropic instability (Vallis 2006). The instability and associated wave generation and growth would lead to changes in wave–mean flow interaction in the affected region, which in turn can lead to changes in wave propagation, dissipation and/or reflection in the high latitudes.

The vertical component $\overline{q}_{\phi,z}$ in the high-latitude upper stratosphere (65°–85°N and 2 hPa; Fig. 7c) also shows greater seasonal variation under HS than LS, with $\overline{q}_{\phi,z}$

approaching zero in December and January and becoming substantially negative in February under HS while remaining primarily positive throughout the winter under LS. Figure 7d indicates that the vertical wind shear $\overline{u}_z$ accounts for the overall reduction of $\overline{q}_{\phi,z}$ but not the oscillation that causes $\overline{q}_{\phi,z}$ to become negative during December and February under HS. It is possible that $\overline{u}_z$ has already become negative in the high-latitude lower mesosphere in November under HS, and the effect then descends into the upper stratosphere from mid-December and remains until mid-January. As a result, vertically
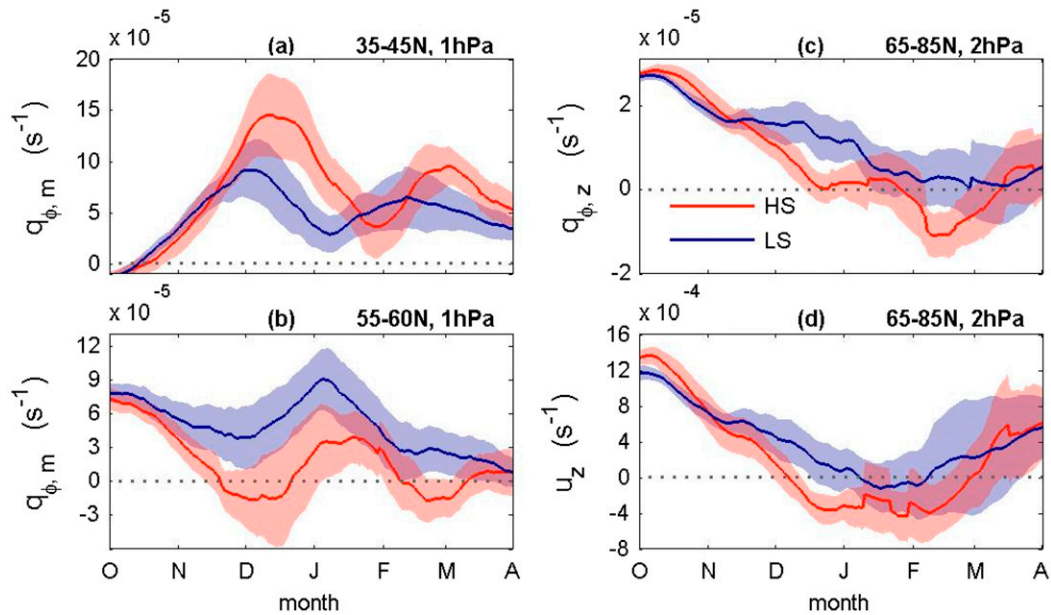
FIG. 7. The 31-day running averages of $\overline{q}_{\phi,m}$ at (a) 35°–40°N and 1 hPa and (b) 55°–60°N and 1 hPa and (c) $\overline{q}_{\phi,z}$ and (d) $\overline{u}_z$ at 65°–85°N and 2 hPa. The blue and red solid lines represent the mean values under HS and LS conditions, respectively, while the shaded regions represent the 95% confidence intervals of the mean.

propagating planetary waves are more likely to be trapped or reflected there under HS from mid-November to mid-January. Also, planetary wave propagation in the extratropical upper stratosphere would be more confined by the negative $\overline{q}_{\phi,m}$ at 55°–60°N and the negative $\overline{q}_{\phi,z}$ poleward of 65°N during the time, promoting enhanced wave amplitude growth in the region under HS conditions.

To assess whether or not these waveguide anomalies in the upper stratosphere are artifacts resulting from the chosen reanalysis dataset, we repeated the same analysis of Fig. 7 using the Japanese 55-year Reanalysis (JRA-55), NASA's Modern-Era Retrospective Analysis for Research and Applications (MERRA), and the NCEP Climate Forecast System Reanalysis (CFSR). Qualitatively similar results were found (not shown). Thus, despite relatively large reanalysis data uncertainty in the upper stratosphere, we find that the solar-induced upper-level waveguide anomalies are rather robust across all four major modern reanalysis products.

c. Changes in E–P flux and divergence

Results presented in section 3b suggest that solar cycle modulation of northern winter PV gradients is confined mostly to the upper stratosphere. However, these waveguide anomalies represent only the necessary, but not the sufficient, conditions for downward wave reflection. In this section, the associated changes in the E–P flux and divergence are examined in order to provide more direct evidence for solar-induced downward wave reflection.

Figure 8a shows the climatological-mean distribution of the total E–P flux $\mathbf{F}$ and divergence $\nabla \cdot \mathbf{F}$ during October–January. They are characterized by upward and equatorward E–P fluxes and their overall convergence (i.e., regions with negative $\nabla \cdot \mathbf{F}$) peaks in the subtropical upper troposphere, the midlatitude midtroposphere, and the extratropical upper stratosphere. Positive values of $\nabla \cdot \mathbf{F}$, indicative of wave generation via instability, are found only in a couple of isolated small regions.

Solar-induced changes in the E–P fluxes during early to midwinter are mainly marked by enhanced poleward E–P flux anomalies in the upper stratosphere and poleward and downward E–P flux anomalies below 5 hPa and poleward of 55°N (Figs. 8b–d). These E–P flux anomalies initiate in the lower-latitude upper stratosphere during October–November, indicating reduced poleward momentum fluxes and/or enhanced poleward wave refraction under HS. They are accompanied by a dipole anomaly of $\nabla \cdot \mathbf{F}$ in height, with strengthened convergence above 3 hPa and reduced convergence below at 3–7 hPa. These upper-level E–P flux and divergence anomalies move poleward with time and become most significant during November–December. However, a downward descent of E–P flux divergent anomalies cannot be clearly identified because of enhanced equatorward E–P flux anomalies in December–January. These stratospheric E–P flux and divergence anomalies do not correspond with a downward descent of zonal mean wind anomalies from the upper
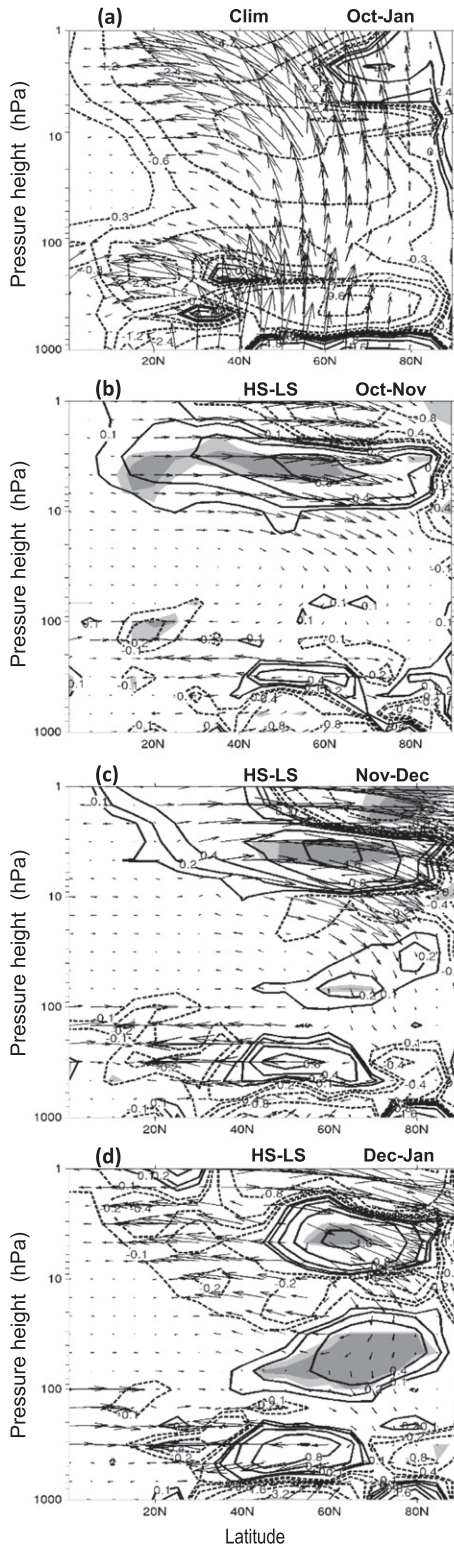
stratosphere to the troposphere (see Figs. 2k–o). The vertical dipole pattern of the $\nabla \cdot \mathbf{F}$ anomalies in the upper stratosphere is nevertheless dynamically consistent with the negative PV gradient anomalies and the negative vertical wind shear $\overline{u}_z$ found in the same region (see Figs. 5, 6). In addition, the downward-pointing E–P flux anomalies appear to be followed, for example, in December–January by increased divergence in the lower stratosphere at 45°–80°N and 30–100 hPa. Thus, the vertical dipole anomaly of $\nabla \cdot \mathbf{F}$ in the high-latitude upper stratosphere and the downward-pointing E–P flux anomalies below are consistent with the presence of a reflecting surface at approximately 3–5 hPa under HS. In the lower to middle troposphere, the composite differences are barely significant at the $p \leq 0.1$ level.

To examine what has led to the positive $\nabla \cdot \mathbf{F}$ anomaly at approximately 3–5 hPa, Fig. 9 shows the temporal evolution of monthly mean quasigeostrophic E–P flux divergence $\nabla \cdot \mathbf{F}_{qg}$ at 45°–60°N and 3–5 hPa (Fig. 9a) and at 65°–75°N and 3–5 hPa (Fig. 9b) from September to March for both HS and LS conditions. We chose to plot $\nabla \cdot \mathbf{F}_{qg}$ instead of the full $\nabla \cdot \mathbf{F}$ because it is most affected by changes in planetary wave activity and it accounts for most of the solar signal in $\nabla \cdot \mathbf{F}$ shown in Fig. 8. The E–P flux divergence $\nabla \cdot \mathbf{F}_{qg}$ at 45°–60°N and 3–5 hPa is generally characterized by an increase in wave convergence from $\nabla \cdot \mathbf{F}_{qg} \approx 0 \, \mathrm{kg \, s^{-2} \, m^{-1}}$ in September to $\nabla \cdot \mathbf{F}_{qg} \leq -1 \, \mathrm{kg \, s^{-2} \, m^{-1}}$ (equivalent to approximately $-8 \, \mathrm{m \, s^{-1} \, day^{-1}}$) in midwinter (December–January) and then a decrease in wave convergence from midwinter to late March under both HS and LS conditions. The solar cycle modulation of $\nabla \cdot \mathbf{F}_{qg}$ is marked by a significantly delayed and deeper development of the wave convergence from September to December under HS. Reduced wave forcing under HS in early winter is consistent with

---

November–December, and December–January mean, respectively. Note that the E–P fluxes are scaled because the vertical flux $F^{(z)}$ becomes vanishingly small with altitude as a result of the decrease in density. The scaling of the form $\{\tilde{F}^{(\phi)}, \tilde{F}^{(z)}\} = (p_s/p)^{0.85}\{F^{(\phi)}/a\pi, F^{(z)}/6 \times 10^5\}$ is applied to the E–P flux climatology, and an additional factor of 10 is applied to the solar cycle differences. Also, the E–P flux divergence is displayed as $\nabla \cdot \tilde{\mathbf{F}} = \nabla \cdot \mathbf{F}/\rho_0 a \cos\phi$ so that the wave forcing has the same units $(\mathrm{m \, s^{-1} \, day^{-1}})$ as the zonal wind tendency in the momentum budget equation (Andrews et al. 1987). Solid and dashed contours are positive and negative divergence, respectively, at the intervals of $\pm 0.3, \pm 0.6, \pm 1.2, \pm 2.4, \ldots \times 10^{-5} \, \mathrm{m \, s^{-1} \, day^{-1}}$ for climatology and $\pm 0.1, \pm 0.2, \pm 0.4, \pm 0.8 \ldots \times 10^{-5} \, \mathrm{m \, s^{-1} \, day^{-1}}$ for the difference plots. The light and dark gray-shaded areas represent the p value ≤ 0.1 and 0.05, respectively.

FIG. 8. (a) The October–January climatological-mean E–P fluxes (arrows) and E–P flux divergence (contours) in latitude–height cross sections of 0°–90°N and 1000–1 hPa. (b)–(d) As in (a), but for solar composite differences (HS − LS) for the October–November,
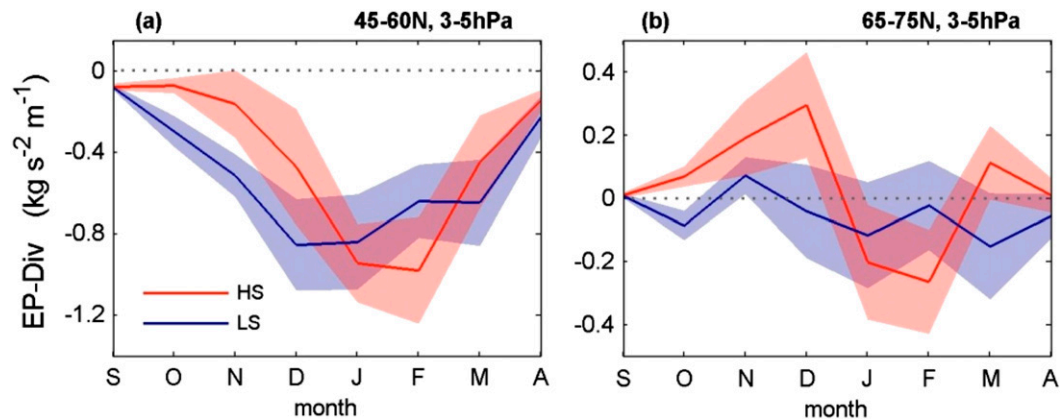
FIG. 9. September–March mean $\nabla \cdot \mathbf{F}_{qg}$ at (a) 45°–60°N and 3–5 hPa and (b) 65°–75°N and 3–5 hPa. The red and blue lines are for the HS and LS conditions, respectively, and the associated color shadings indicate the 95% confidence intervals.

enhanced westerlies in the lower latitude upper strato-sphere (see Figs. 2k,l).At high latitudes (i.e., 65°–75°N and 3–5 hPa), the solar cycle modulation of $\nabla \cdot \mathbf{F}_{qg}$ is marked by greater seasonal variation under HS (and vice versa under LS), during that time $\nabla \cdot \mathbf{F}_{qg}$ remains mostly negative except for November. The increased seasonal variation under HS is marked by the absolute value of $\nabla \cdot \mathbf{F}_{qg}$ being positive in early winter and in March, but negative in January to February. The positive $\nabla \cdot \mathbf{F}_{qg}$ indicates Rossby wave generation via instability, con-sistent with increased occurrence of $\overline{q}_{\phi,m} \leq 0$ at about 55°–60°N and 1 hPa under HS (Fig. 7b). This localized instability would lead to enhanced momentum transfer from the background zonal-mean flow to wave activity and therefore plays a role in inducing the negative shear in the extratropical upper stratosphere. On the other hand, the negative $\nabla \cdot \mathbf{F}_{qg}$ in January–February under HS indicates enhanced wave dissipation, which is also dy-namically consistent with an overall $\overline{q}_{\phi} \leq 0$. The reversal of $\nabla \cdot \mathbf{F}_{qg}$ from positive to negative in January–February is also consistent with the zonal mean wind and temperature anomalies (see Fig. 2). As a whole, Fig. 9 indicates that the delayed seasonal development of $\nabla \cdot \mathbf{F}_{qg}$ at 45°–60°N and 3–5 hPa under HS is accompanied by enhanced Rossby wave generation around December and stronger wave breaking in January–February in the high latitudes.

d. Evidence of downward wave reflection

Previous studies have indicated that positive $\nabla \cdot \mathbf{F}$ and wave generation near the reflecting surface are the cri-teria for downward wave reflection (Dunn-Sigouin and Shaw 2015). Results from the previous sections have suggested that reflecting surfaces are more likely to form in the high-latitude upper stratosphere under HS during November–January. During this time, a vertical dipole

pattern of $\nabla \cdot \mathbf{F}$ anomalies is found in the extratropics near 2–3 hPa with poleward- and downward-pointing E–P flux anomalies below (Fig. 8). Furthermore, the positive $\nabla \cdot \mathbf{F}$ anomalies at high latitudes are solely due to the contribution from HS winters. In this section, we provide further evidence to demonstrate that downward reflection of planetary waves contributes to these downward E–P flux anomalies.

Figure 10 shows the seasonal progression of the climatology and solar composite differences (HS − LS) of the wave-2 heat flux $\overline{v'T'}$ (Figs. 10a–c) during November–December and the corresponding difference in the average number of days when negative wave-2 heat flux $\overline{v'T'}$ occurred (Figs. 10d,e,f). The solar differ-ences of $\overline{v'T'}$ are marked by a dipole pattern in the upper stratosphere with significant negative anomalies pole-ward of 55°N and positive anomalies at 20°–40°N. Be-cause they are located on the poleward and equatorward flanks of the $\overline{v'T'}$ climatology, this pair of anomalies indicates an equatorward shift of $\overline{v'T'}$ under HS, in agreement with the PV gradient anomalies (see Fig. 6). As the winter progresses into midwinter, the region with negative $\overline{v'T'}$ anomalies expands gradually towards the surface (Figs. 10b,c).

A more direct criterion for downward wave reflection is the presence of negative daily heat fluxes somewhere between the reflecting surface and the ground (Harnik and Lindzen 2001; Dunn-Sigouin and Shaw 2015). Indeed, the seasonal mean $\overline{v'T'}$ anomalies during November–December are accompanied by significantly increased occurrence of negative daily $\overline{v'T'}$ poleward of 60°N and significantly reduced occurrence of negative daily $\overline{v'T'}$ at 20°–40°N, 10–3 hPa (Figs. 10d–f). It is clear that the high-latitude negative $\overline{v'T'}$ occurrence anomalies tend to peak near the region with the dipole anomalies of $\nabla \cdot \mathbf{F}$ (see
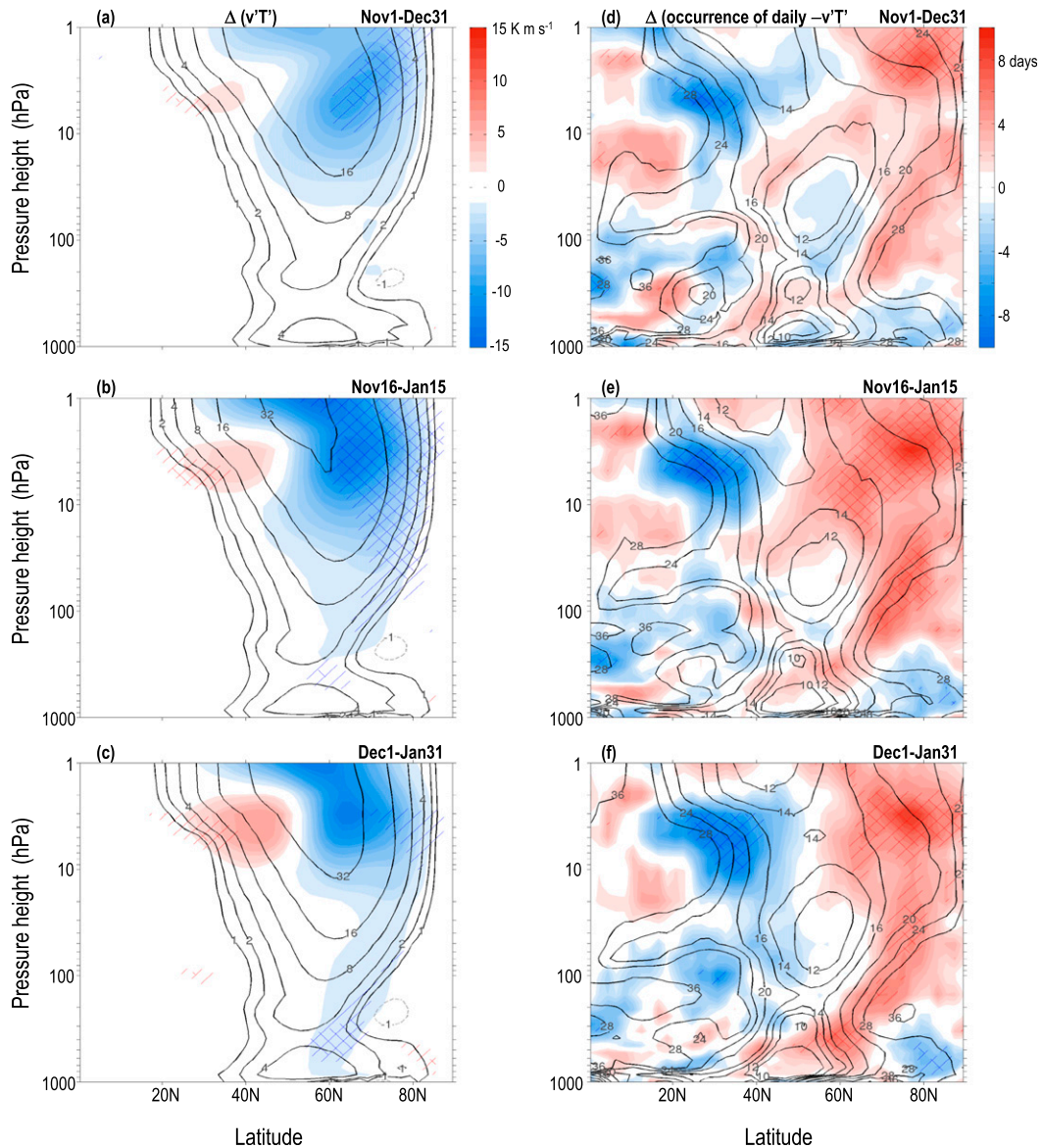
FIG. 10. Climatology (contours) and solar composite differences (HS − LS; shaded) of wave-2 heat flux $\overline{v'T'}$ for a 61-day period starting from (a),(d) 1 Nov, (b),(e) 16 Nov, and (c),(f) 1 Dec for (a)–(c) seasonal mean and (d)–(f) the number of days during which negative daily wave-2 $\overline{v'T'}$ occurred. The backward and forward hatches indicate that the differences are statistically significant at p values ≤ 0.1 and 0.05, respectively.

Fig. 8b–d). We find that these upper-level negative $\overline{v'T'}$ occurrence anomalies, however, do not propagate directly into the troposphere. Instead, they indicate reduced upward wave-2 propagation and contribute to the formation of the reflecting surface in the upper stratosphere. The enhanced downward wave-2 reflections, in fact, take place at and below 10 hPa. The effects start around mid-November and last until late January.

These seasonal mean $\overline{v'T'}$ anomalies are accompanied by significantly increased occurrence of negative daily $\overline{v'T'}$ poleward of 60°N and significantly reduced occurrence of negative daily $\overline{v'T'}$ at 20°–40°N, 10–3 hPa (Figs. 10d–f), implying persistently enhanced upward wave propagation in this region. This agrees with the positive anomalies of $\overline{q}_\phi$ above 1–2 hPa as waves are guided to propagate toward the region with larger values of $\overline{q}_\phi$ (Vallis 2006). In high latitudes, the negative $\overline{v'T'}$ occurrence anomalies first appear near the region with the vertical dipole anomaly of $\nabla \cdot \mathbf{F}$ (see Figs. 8b–d). Additional negative $\overline{v'T'}$ occurrence anomalies then appear below 10 hPa and spread downward with time, implying enhanced downward wave-2 reflection.

Figure 11 shows the seasonal evolution of the climatological stationary wave 2 under HS (color contours) and LS conditions (black contours) (Fig. 11, left) and the corresponding differences (HS − LS) (Fig. 11, right) during October–January. They are estimated using 61-day mean geopotential height with a time interval of 15 days between the adjacent panels (top to bottom), all averaged over the latitude band 65°–85°N and displayed in a longitude–height cross section.

Under both HS and LS, the climatological wave 2 has peak amplitude in the midstratosphere, a westward phase tilt with height in the stratosphere and slightly eastward phase tilt in the troposphere. Solar cycle modulation of these waves (Fig. 11, right) is marked by a significant reduction of wave activity in the upper stratosphere in October–November. As time progresses, these upper-level wave amplitude anomalies descend to lower levels, and the phase of the anomalies gradually tilts eastward with height. From December, the anomalies emerge in the lower troposphere and form a standing wave-2 pattern with height, suggesting an enhanced interference between upward- and downward-propagating waves. These wave-2 anomalies support the idea that downward wave reflection occurs more frequently under HS than under LS. The wave anomalies are associated with a downward movement as well as more eastward-tilted phase with height, which is known to link to a downward group velocity (Harnik and Lindzen 2001). It is worth noting that the wave anomalies presented here are 61-day averages only to show the statistical differences between HS and LS conditions, whereas individual downward reflection events are more episodic and lasted a few days only.

Figures 12a and 12b show the longitude–latitude display of November–December mean stationary wave-2 climatology (shaded) and solar composite difference (contours) at 10 and 50 hPa, respectively. Similar results can be obtained at other stratospheric levels (not shown). The solar signal in stratospheric wave 2 is shifted approximately 45° eastward with respect to the climatological wave 2. The amplitudes of the anomalies are up to 80, 60, and 35 m in the upper, middle, and lower stratospheres. They represent 40%, 30%, and 15% of the corresponding climatological wave-2 amplitude at the given levels. These percentage changes are not only statistically significant but also substantially larger than those associated with zonal mean anomalies.

Figure 12c is as in Figs. 12a,b, but for the November–January mean at 850 hPa. Similar but slightly weaker signals can be found at other tropospheric levels (not shown). The solar signal in the tropospheric wave 2 is confined to the high latitudes, and the phase of the anomalies is clearly shifted from climatology, indicating wave reflection instead of simple wave reduction. The amplitude of these wave-2 anomalies at 850 hPa is about 8 m, which is comparable to about 15% of its climatological mean at the affected latitudes.

Downward reflection of wave 1 is also found to be enhanced under HS. Figure 13 shows the behavior of planetary wave-1 anomalies at 500 and 850 hPa from mid-November to early January. At both pressure levels, the geopotential wave-1 anomalies first appear poleward of 80°N around mid-November. The signal then gradually expands equatorward and westward to midlatitudes until early January, when the differences reach a maximum amplitude of 32 m at 500 hPa and 24 m at 850 hPa. At 500 hPa, the wave-1 anomalies are comparable both in phase and in amplitude to those estimated from downward wave-1 reflected events, although the solar-induced wave-1 anomalies appear to be more confined to higher latitudes [see Fig. 10 of Shaw and Perlwitz (2013)]. In comparison with solar-induced wave-2 anomalies (Fig. 12c), the wave-1 anomalies appear earlier around mid-November, are relatively short-lived, and are confined to higher latitudes. In addition, both wave-1 and wave-2 anomalies follow a similar transient behavior, with the tropospheric anomalies periodically extending to lower latitudes (not shown).

4. Conclusions and discussion

The analysis described above has shown that the 11-yr solar cycle significantly modulates the potential vorticity (PV) gradients in the upper stratosphere during NH winter. Under HS, the effect is marked by enhanced PV gradients on the equatorward flank of the westerly jet and reduced PV gradient on its poleward flank. These midlatitude PV gradient anomalies are present throughout the entire NH winter, but their effects are most pronounced during November–December, when the upper-level polar-night jet westerlies are strongest. In addition, small or negative PV gradients and negative vertical wind shears are more likely to develop in the high-latitude upper stratosphere in November–January under HS. The corresponding changes in the E–P fluxes and divergence are characterized by enhanced poleward wave focusing from the westerly jet region. These upper-level E–P flux anomalies are accompanied by E–P flux convergent anomalies above 3 hPa and divergent anomalies at approximately 5 hPa. Downward and poleward E–P flux anomalies are diagnosed below the dipole anomaly of $\nabla \cdot \mathbf{F}$, and the effect gradually extends from the upper stratosphere into the lower troposphere during December–January. These E–P flux anomalies are consistent with waveguide anomalies in the same region (see
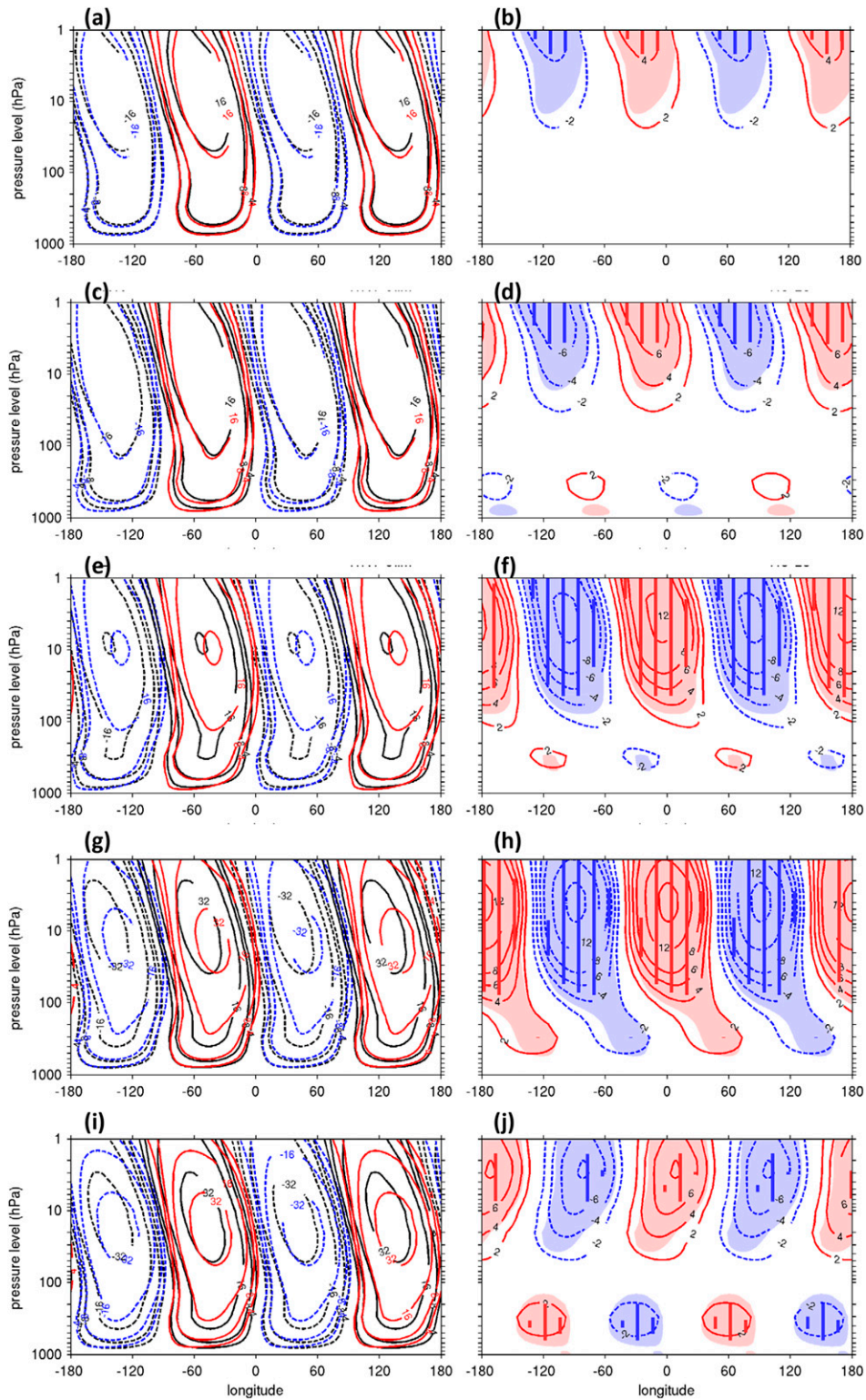
FIG. 11. Longitude–height cross section of the climatology of stationary wave 2 under HS (color contours) and LS (black contours) estimated from geopotential height averaged over the latitude band of 65°–85°N and a 61-day period starting from (a) 1 Oct, (c) 16 Oct, (e) 1 Nov, (g) 16 Nov, and (i) 1 Dec The contours are ±2, ±4, ±8, ±16, and ±32 m. (b),(d),(f),(h),(j) Corresponding solar cycle composite differences, where the contours are ±2, ±4, ±8, ±12, and ±16 m. The shadings and the vertical thick lines indicate the differences are statistically significant at the p value ≤ 0.1 and 0.05, respectively.
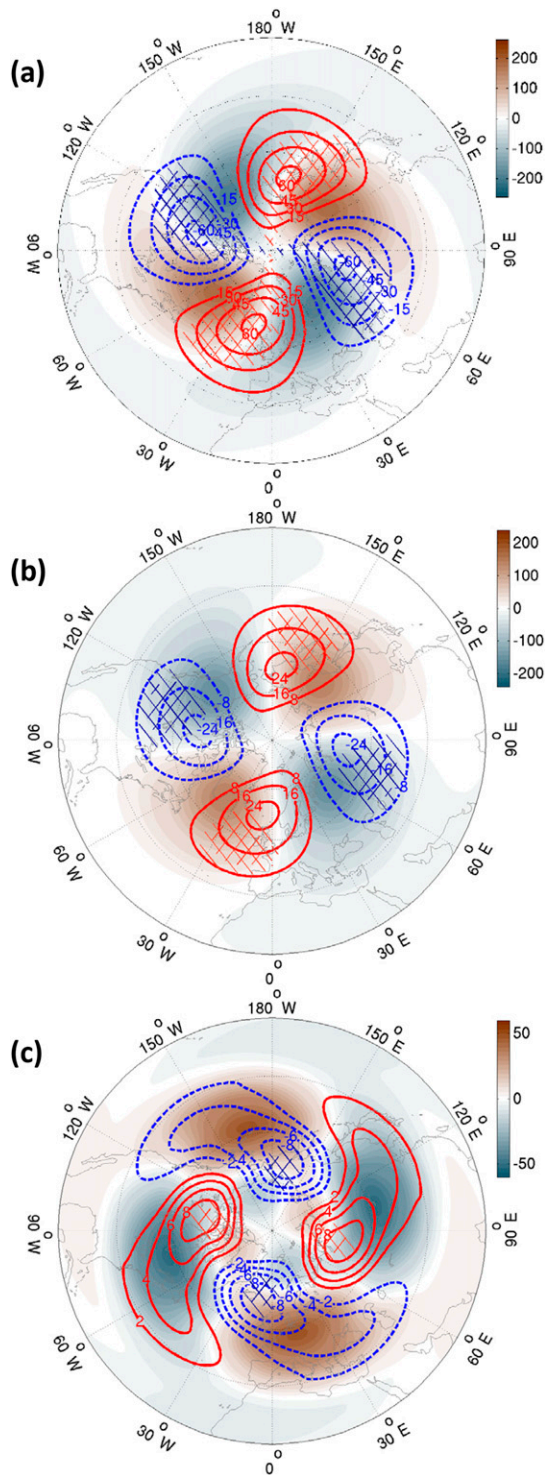
FIG. 12. Longitude–latitude (20°–90°N) cross section of the NH climatology (shaded) and anomalies (HS − LS; contours) of wave-2 geopotential for November–December averages at (a) 10 and (b) 50 hPa. (c) As in (a),(b), but for November–January mean at 850 hPa. The contour intervals for (a)–(c) are 15, 8, and 2 m, respectively. The forward and backward hatches indicate the p value ≤ 0.1 and 0.05, respectively.

Figs. 5–7) and correspond well with enhanced downward reflection of planetary wave 2 (Figs. 10–12).

A region with strengthened meridional curvature in the profile of zonal mean zonal wind causes the horizontal component of the meridional PV gradient $\overline{q}_{\phi,m}$ to become negative more frequently under HS. A condition for barotropic instability, $\overline{q}_{\phi,m} \leq 0$, was accompanied by positive Rossby wave E–P flux divergence at higher latitudes (Fig. 9b). These upper-level anomalies may also affect the ''surf zone,'' a region where planetary wave breaking could lead to nonlinear wave breaking and reflection (McIntyre 1982). If this occurs, the wave generation via instability and poleward reflection would lead to a positive feedback and, consequently, an enhanced separation between the waveguides in the subtropics and at high latitudes. Such an interpretation is consistent with the PV anomalies shown in section 3b.

We propose the following sequential steps as an aid to explaining the observed downward wave reflection under HS. They consist of four distinct components, as shown in Fig. 14:

1) Enhanced solar UV radiation and ozone heating leads to a warmer tropical stratopause, a steeper meridional temperature gradient, and thus a stronger westerly jet in the subtropical lower mesosphere and upper stratosphere.

2) The enhanced westerly jet induces changes in the latitudinal curvature of $\overline{u}$ with enhanced PV gradient at the equatorward flank of the jet and more frequent occurrence of negative PV gradient on its poleward flank. These changes in wave geometry cause poleward wave refraction from the jet core as well as wave generation via barotropic instability at 55°–60°N, leading to a further strengthening of the subtropical westerlies and the westerly winds in the mid-to-high-latitudes in the middle stratosphere.

3) The development of a surf zone at 1–2 hPa and above on the poleward flank of the subtropical westerly jet, where a negative PV gradient exists, also leads to nonlinear wave–mean flow interaction. Upward-propagating waves from below experience wave growth in amplitude as a result of conservation of wave activity. These waves then break in the region between the pole and the surf zone, causing deceleration of the winds.

4) The combined effects of 2 and 3 above lead to a region of negative vertical shear $\overline{u}_z$ and the formation of a reflecting surface in the high-latitude upper stratosphere. Enhanced downward wave reflection takes place below the reflecting surface.

Given that the signals are initialized in the region where solar UV is known to have a direct effect, we
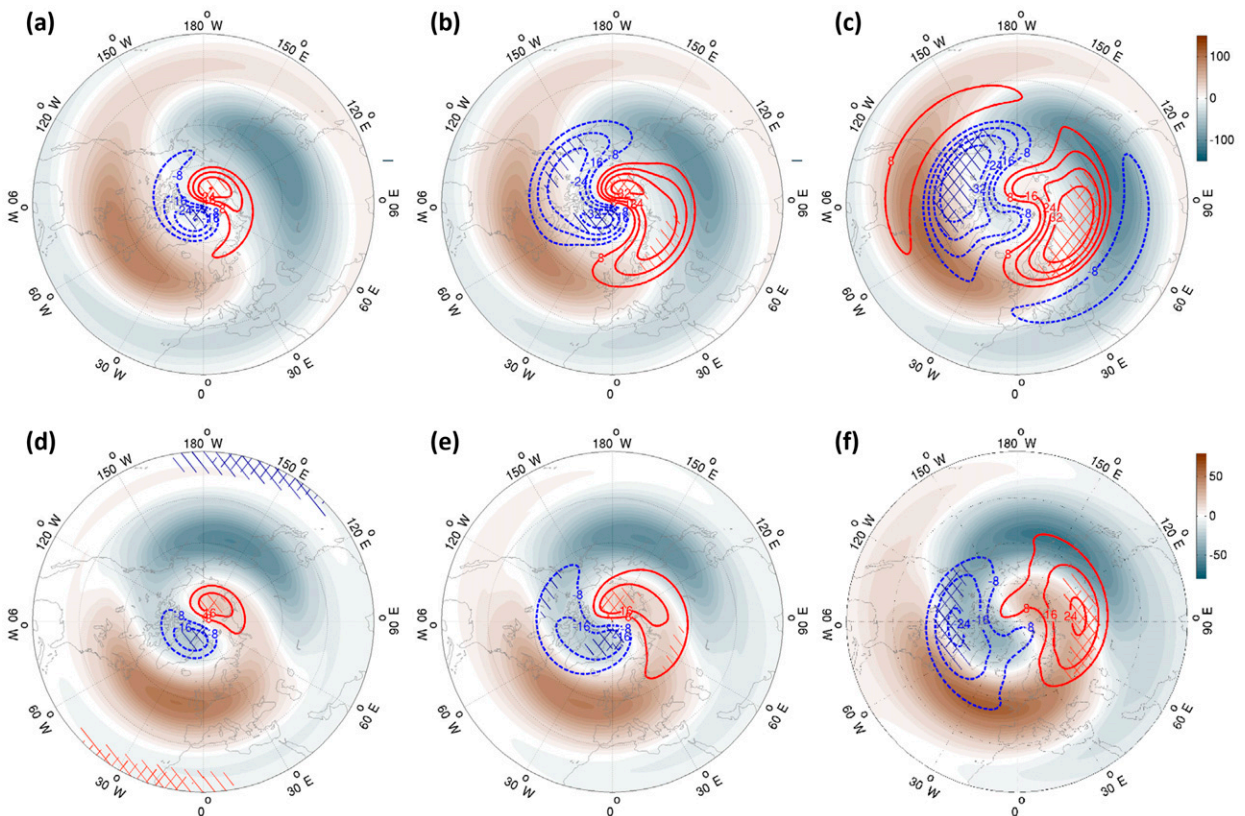
FIG. 13. Longitude–latitude (20°–90°N) cross section of the climatology (shaded; m) and solar differences (HS − LS; contours with an interval of ±8 m) of geopotential wave 1 at (a)–(c) 500 hPa and at (d)–(f) 850 hPa for 31-day averages starting from (a),(d) 16 and (b),(e) 26 Nov and (c),(f) 6 Dec. The forward and backward hashed regions indicate the p value ≤ 0.1 and 0.05, respectively.

suggest that the signals represent dynamic response to solar UV forcing in the upper stratosphere and lower mesosphere. This new "top down" pathway via wave reflection appears to be most effective when the initial state of the stratosphere is less disturbed. This is because the development of the barotropic instability and a nonlinear surf zone requires a stable jet as well as initial small wave forcing from below (McIntyre 1982). These conditions appear to be best met in November–December (Figs. 2k,l) under HS. However, they are likely to break down under either HS or LS conditions after December, when the upward propagating planetary waves from the troposphere become intense. This may explain why the solar-induced downward wave reflection is most significant around December.

Previous studies showed that a vertical reflecting surface formed in the northern upper stratosphere in either November–December or February–March, but significant downward reflection occurred only during the late period (Perlwitz and Harnik 2003, 2004; Shaw et al. 2010; Shaw and Perlwitz 2013). It was shown that, in February–March, the wave reflection events led to

significant tropospheric anomalies that resemble a positive NAO (Shaw and Perlwitz 2013). The lack of downward reflection in early winter was attributed previously to a wide stratospheric meridional waveguide and stronger wave absorption in the vicinity of the subtropical zero-wind line in the middle stratosphere. Here, we demonstrated that the wave geometry measured by the PV gradient for downward reflection of stationary waves is enhanced under HS around December and February. However, solar-induced downward reflection differs in character from those earlier studies on climatological reflection events. First, solar-induced downward reflection is only detected around December, not in February. The lack of late winter signal is probably due to enhanced wave dissipation in the upper stratosphere, which is indicated by Figs. 2n,o. Second, solar-induced downward reflection is found to be primarily associated with wave 2, while late winter reflection events were associated with wave 1. Under HS, the reflection of wave 2 is significantly enhanced from November to January, while wave-1 reflection is relatively short-lived, occurring briefly only around
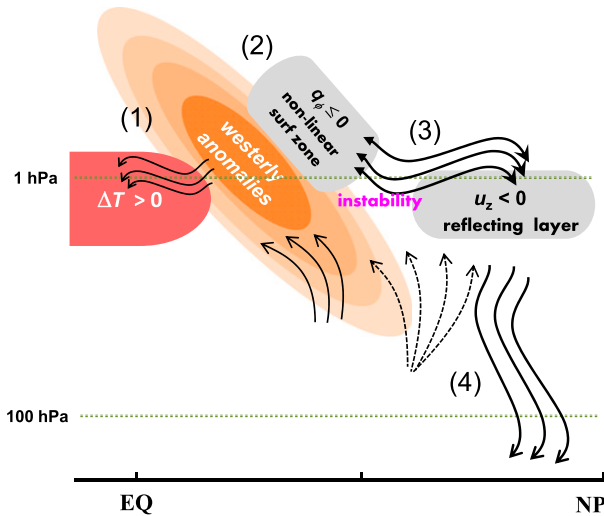
FIG. 14. Schematic diagram showing the sequence (from 1 to 4) that leads to downward wave reflection and tropospheric changes due to enhanced solar UV forcing. The red half oval represents solar UV enhanced temperature anomalies, while orange ovals indicate westerly wind anomalies. The gray-shaded regions represent reflecting and critical layers where nonlinear wave breaking, reflection, and/or overreflection occur. The thick solid and thin dashed arrows indicate enhanced and reduced planetary wave propagation, respectively, while the curves with the arrows in both ends indicate wave reflection and breaking. The region where barotropic instability occurs is also highlighted. See text for further details.

December. In the troposphere, the reflected wave-1 anomalies are more confined to the high-latitude areas, while the wave-2 anomalies are found in mid-latitudes. Finally, the solar-induced downward-reflected waves, especially wave-1 anomalies, do not appear to project onto the NAO directly, while the late winter wave-1 reflection events appear to have an immediate effect on the NAO. Further studies are needed to understand the extent to which solar-induced downward reflection is linked to the positive NAO signal in January–February (Fig. 3) and the negative geopotential height anomalies in the Arctic from mid-November to mid-February (Fig. 4).

There is a slight mismatch between the timing of the wave-2 reflection and that of waveguide changes (Figs. 7c,d). This might be because the waveguide diagnostics are suited strictly for stationary waves, while other diagnostics are suited for all waves. Downward reflection of transient waves would have different wave geometry to those presented in Fig. 5, because of a nonlinear coupling among the PV gradient $\overline{q}_\phi$, the zonal mean wind speed $\overline{u}$, and the phase speed c via the term $\overline{q}_\phi/(\overline{u} - c)$ (Charney and Drazin 1961). During the time when and at the places where meridional wave reflection and/or transient wave

activity play a major role, it becomes harder to separate the signal of downward reflection of stationary waves and solar modulation of transient wave activity. Nevertheless, this complexity does not affect the main conclusion of this paper. That is, downward wave reflection is enhanced under HS from early winter to midwinter.

Changes in absorption or reflection near the critical line could affect the transient wave activity, which may also play a role in the solar-induced downward reflection. Resonance may arise when transient waves are trapped either meridionally or vertically (Tung and Lindzen 1979a,b). Significant reflection from the critical line and regions with strong westerlies may result in sudden stratospheric warmings (SSWs) (Plumb 1981). Our results suggest a more confined cavity for wave propagation to associate with HS winters, which may act to precondition the background flow and lead to a more disturbed polar vortex in late winter. Such a response is, in fact, found in February and March (Figs. 2n,o). A warmer upper-stratospheric polar vortex in late winter was reported previously using other reanalysis datasets (i.e., Lu et al. 2009; Mitchell et al. 2014). A reversal of E–P flux divergent anomalies in late winter has also been seen in model studies (i.e., Ineson et al. 2011; Mitchell et al. 2015). This may explain the lack of solar-induced downward wave reflection signal in February, while a suitable wave geometry is found in the upper stratosphere (Figs. 7c,d). In addition, the late winter reversal could lead to different or even opposing responses in the troposphere. This may explain why there is generally weaker or even a lack of a solar signal in climate model simulations, especially when the assessment is made based on midwinter averages.

We are aware that the presence of other decadal variations in the climate system could also contribute to significant differences between high and low solar winters. In particular, the tropospheric solar signal may be affected by additional processes (such as SST feedbacks). Because the length of the data employed by this study, covering only three solar cycles (i.e., 1979–2013), a credible assessment of contamination and/or amplification by other processes cannot be made. Finally, it is important that the proposed new mechanism is checked across other reanalysis datasets for its robustness and validated by model simulations.

Programme (GA01101) and the European Union Framework 7 SPECS project. The paper has benefited from the constructive suggestions of three anonymous reviewers. We acknowledge use of ECMWF interim reanalysis datasets (http://apps.ecmwf.int/datasets/data/interim-full-daily). We thank Tony Philips for help with acquiring and managing the ERA-Interim data.

REFERENCES

Andrews, D. G., J. R. Holton, and C. B. Leovy, 1987: *Middle Atmosphere Dynamics.* International Geophysics Series, Vol. 40, Academic Press, 489 pp.

Andrews, M. B., J. R. Knight, and L. J. Gray, 2015: A simulated lagged response of the North Atlantic Oscillation to the solar cycle over the period 1960–2009. *Environ. Res. Lett.*, **10**, 054022, doi:10.1088/1748-9326/10/5/054022.

Balachandran, N. K., D. Rind, P. Lonergan, and D. T. Shindell, 1999: Effects of solar cycle variability on the lower stratosphere and the troposphere. *J. Geophys. Res.*, **104**, 27 321–27 339, doi:10.1029/1999JD900924.

Brasseur, G. P., and S. Solomon, 2005: *Aeronomy of the Middle Atmosphere.* Atmospheric and Oceanographic Sciences Library, Vol. 32, D. Reidel Publishing Company, 646 pp., doi:10.1007/1-4020-3824-0.

Charney, J. G., and P. G. Drazin, 1961: Propagation of planetary scale disturbances from the lower into the upper atmosphere. *J. Geophys. Res.*, **66**, 83–109, doi:10.1029/JZ066i001p00083.

Chiodo, G., N. Calvo, D. R. Marsh, and R. Garcia-Herrera, 2012: The 11-year solar cycle signal in transient simulations from the Whole Atmosphere Community Climate Model. *J. Geophys. Res.*, **117**, D06109, doi:10.1029/2011JD016393.

——, D. Marsh, R. Garcia-Herrera, N. Calvo, and J. Garca, 2014: On the detection of the solar signal in the tropical stratosphere. *Atmos. Chem. Phys.*, **14**, 5251–5269, doi:10.5194/acp-14-5251-2014.

Cnossen, I., H. Lu, C. J. Bell, L. J. Gray, and M. M. Joshi, 2011: Solar signal propagation: The role of gravity waves and stratospheric sudden warmings. *J. Geophys. Res.*, **116**, D02118, doi:10.1029/2010JD014535.

Dee, D. P., and S. Uppala, 2009: Variational bias correction of satellite radiance data in the ERA-Interim reanalysis. *Quart. J. Roy. Meteor. Soc.*, **135**, 1830–1841, doi:10.1002/qj.493.

——, and Coauthors, 2011: The ERA-Interim reanalysis: Configuration and performance of the data assimilation system. *Quart. J. Roy. Meteor. Soc.*, **137**, 553–597, doi:10.1002/qj.828.

de Toma, G., O. R. White, B. G. Knapp, G. J. Rottman, and T. N. Woods, 1997: Mg II core-to-wing index: Comparison of SBUV2 and SOLSTICE time series. *J. Geophys. Res.*, **102**, 2597–2610, doi:10.1029/96JA03342.

Dunn-Sigouin, E., and T. A. Shaw, 2015: Comparing and contrasting extreme stratospheric events, including their coupling to the tropospheric circulation. *J. Geophys. Res. Atmos.*, **120**, 1374–1390, doi:10.1002/2014JD022116.

Frame, T. H. A., and L. J. Gray, 2010: The 11-yr solar cycle in ERA-40 data: An update to 2008. *J. Climate*, **23**, 2213–2222, doi:10.1175/2009JCLI3150.1.

Gray, L. J., S. Crooks, C. Pascoe, S. Sparrow, and M. Palmer, 2004: Solar and QBO influences on the timing of stratospheric sudden warmings. *J. Atmos. Sci.*, **61**, 2777–2796, doi:10.1175/JAS-3297.1.

——, and Coauthors, 2010: Solar influences on climate. *Rev. Geophys.*, **48**, RG4001, doi:10.1029/2009RG000282.

——, and Coauthors, 2013: A lagged response to the 11 year solar cycle in observed winter Atlantic/European weather patterns. *J. Geophys. Res. Atmos.*, **118**, 13 405–13 420, doi:10.1002/2013JD020062.

——, T. J. Woollings, M. Andrews, and J. Knight, 2016: Eleven-year solar cycle signal in the NAO and Atlantic/European blocking. *Quart. J. Roy. Meteor. Soc.*, **142**, 1890–1903, doi:10.1002/qj.2782.

Haigh, J. D., 1994: The role of stratospheric ozone in modulating the solar radiative forcing of climate. *Nature*, **370**, 544–546, doi:10.1038/370544a0.

——, R. Blackburn, and R. Day, 2005: The response of tropospheric circulation to perturbations in lower-stratospheric temperature. *J. Climate*, **18**, 3672–3685, doi:10.1175/JCLI3472.1.

Harnik, N., and R. S. Lindzen, 2001: The effect of reflecting surfaces on the vertical structure and variability of stratospheric planetary waves. *J. Atmos. Sci.*, **58**, 2872–2894, doi:10.1175/1520-0469(2001)058<2872:TEORSO>2.0.CO;2.

Hines, C. O., 1974: A possible mechanism for the production of sun-weather correlations. *J. Atmos. Sci.*, **31**, 589–591, doi:10.1175/1520-0469(1974)031<0589:APMFTP>2.0.CO;2.

Hood, L. L., 2004: Effects of solar UV variability on the stratosphere. *Solar Variability and Its Effects on Climate*, J. M. Pap et al, Eds., Amer. Geophys. Union, 283–303, doi:10.1029/141GM20.

——, and B. E. Soukharev, 2012: The lower-stratospheric response to 11-yr solar forcing: Coupling to the troposphere–ocean response. *J. Atmos. Sci.*, **69**, 1841–1863, doi:10.1175/JAS-D-11-086.1.

——, and Coauthors, 2015: Solar signals in CMIP-5 simulations: The ozone response. *Quart. J. Roy. Meteor. Soc.*, **141**, 2670–2689, doi:10.1002/qj.2553.

Ineson, S., A. A. Scaife, J. R. Knight, J. C. Manners, N. J. Dunstone, L. J. Gray, and J. D. Haigh, 2011: Solar forcing of winter climate variability in the Northern Hemisphere. *Nat. Geosci.*, **4**, 753–757, doi:10.1038/ngeo1282.

James, I. N., 1994: *Introduction to Circulation Atmospheres.* Cambridge University Press, 422 pp.

Kidston, J., A. A. Scaife, S. C. Hardiman, D. M. Mitchell, N. Butchart, M. P. Baldwin, and L. J. Gray, 2015: Stratospheric influence on tropospheric jet streams, storm tracks and surface weather. *Nat. Geosci.*, **8**, 433–440, doi:10.1038/ngeo2424.

Kodera, K., 1995: On the origin and nature of the interannual variability of the winter stratospheric circulation in the Northern Hemisphere. *J. Geophys. Res.*, **100**, 14 077–14 087, doi:10.1029/95JD01172.

——, 2002: Solar cycle modulation of the North Atlantic Oscillation: Implication in the spatial structure of the NAO. *Geophys. Res. Lett.*, **29**, 1218, doi:10.1029/2001GL014557.

——, and Y. Kuroda, 2002: Dynamical response to the solar cycle. *J. Geophys. Res.*, **107**, 4749, doi:10.1029/2002JD002224.

Labitzke, K., 1987: Sunspots, the QBO, and the stratospheric temperature in the north polar region. *Geophys. Res. Lett.*, **14**, 535–537, doi:10.1029/GL014i005p00535.

Lockwood, M., R. Harrison, T. Woollings, and S. Solanki, 2010: Are cold winters in Europe associated with low solar activity? *Environ. Res. Lett.*, **5**, 024001, doi:10.1088/1748-9326/5/2/024001.

Lu, H., M. J. Jarvis, H.-F. Graf, P. C. Young, and R. B. Horne, 2007: Atmospheric temperature responses to solar irradiance and geomagnetic activity. *J. Geophys. Res.*, **112**, D11109, doi:10.1029/2006JD007864.

——, L. J. Gray, M. P. Baldwin, and M. J. Jarvis, 2009: Life cycle of the QBO-modulated 11-year solar cycle signals in the

Northern Hemispheric winter. *Quart. J. Roy. Meteor. Soc.*, **135**, 1030–1043, doi:10.1002/qj.419.

——, T. J. Bracegirdle, T. Phillips, and J. Turner, 2015: A comparative study of wave forcing derived from the ERA-40 and ERA-Interim reanalysis datasets. *J. Climate*, **28**, 2291–2311, doi:10.1175/JCLI-D-14-00356.1.

Matthes, K., U. Langematz, L. L. Gray, K. Kodera, and K. Labitzke, 2004: Improved 11-year solar signal in the Freie Universität Berlin Climate Middle Atmosphere Model (FUB-CMAM). *J. Geophys. Res.*, **109**, D06101, doi:10.1029/2003JD004012.

——, Y. Kuroda, K. Kodera, and U. Langematz, 2006: Transfer of the solar signal from the stratosphere to the troposphere: Northern winter. *J. Geophys. Res.*, **111**, D06108, doi:10.1029/2005JD006283.

McIntyre, M. E., 1982: How well do we understand the dynamics of stratospheric warmings? *J. Meteor. Soc. Japan*, **60**, 37–65.

Mitchell, D. M., and Coauthors, 2014: Signatures of naturally induced variability in the atmosphere using multiple reanalysis datasets. *Quart. J. Roy. Meteor. Soc.*, **141**, 2011–2031, doi:10.1002/qj.2492.

——, and Coauthors, 2015: Solar signals in CMIP-5 simulations: The stratospheric pathway. *Quart. J. Roy. Meteor. Soc.*, **141**, 2390–2403, doi:10.1002/qj.2530.

Perlwitz, J., and N. Harnik, 2003: Observational evidence of a stratospheric influence on the troposphere by planetary wave reflection. *J. Climate*, **16**, 3011–3026, doi:10.1175/1520-0442(2003)016<3011:OEOASI>2.0.CO;2.

——, and ——, 2004: Downward coupling between the stratosphere and troposphere: The relative role of wave and zonal mean processes. *J. Climate*, **17**, 4902–4909, doi:10.1175/JCLI-3247.1.

Plumb, R. A., 1981: Instability of the distorted polar night vortex: A theory of stratospheric warmings. *J. Atmos. Sci.*, **38**, 2514–2531, doi:10.1175/1520-0469(1981)038<2514:IOTDPN>2.0.CO;2.

Rozanov, E. V., M. E. Schlesinger, T. A. Egorova, B. Li, N. Andronova, and V. A. Zubov, 2004: Atmospheric response to the observed increase of solar UV radiation from solar minimum to solar maximum simulated by the University of Illinois at Urbana–Champaign climate–chemistry model. *J. Geophys. Res.*, **109**, D01110, doi:10.1029/2003JD003796.

Ruzmaikin, A. and J. Feynman, 2002: Solar influence on a major mode of atmospheric variability. *J. Geophys. Res.*, **107**, ACL 7-1–ACL 7-11, doi:101029/2001JD001239.

Scaife, A. A., J. Austin, N. Butchart, S. Pawson, M. Keil, J. Nash, and I. N. James, 2000: Seasonal and interannual variability of the stratosphere diagnosed from UKMO TOVS analyses. *Quart. J. Roy. Meteor. Soc.*, **126**, 2585–2604, doi:10.1002/qj.49712656812.

——, S. Ineson, J. R. Knight, L. Gray, K. Kodera, and D. M. Smith, 2013: A mechanism for lagged North Atlantic climate response

to solar variability. *Geophys. Res. Lett.*, **40**, 434–439, doi:10.1002/grl.50099.

Schmidt, H., G. P. Brasseur, and M. A. Giorgetta, 2010: Solar cycle signal in a general circulation and chemistry model with internally generated quasi-biennial oscillation. *J. Geophys. Res.*, **115**, D00I14, doi:10.1029/2009JD012542.

Shaw, T. A., and J. Perlwitz, 2013: The Life of Northern Hemisphere downward wave reflection between the stratosphere and troposphere. *J. Climate*, **26**, 1745–1763, doi:10.1175/JCLI-D-12-00251.1.

——, ——, and N. Harnik, 2010: Downward wave reflection between the stratosphere and troposphere: The importance of meridional wave guiding and comparison with zonal-mean coupling. *J. Climate*, **23**, 6365–6381, doi:10.1175/2010JCLI3804.1.

Shepherd, T. G., and T. A. Shaw, 2004: The angular momentum constraint on climate sensitivity and downward influence in the middle atmosphere. *J. Atmos. Sci.*, **61**, 2899–2908, doi:10.1175/JAS-3295.1.

Simpson, I. R., M. Blackburn, and J. D. Haigh, 2009: The role of eddies in driving the tropospheric response to stratospheric heating perturbations. *J. Atmos. Sci.*, **66**, 1347–1365, doi:10.1175/2008JAS2758.1.

Thiéblemont, R., K. Matthes, N. E. Omrani, K. Kodera, and F. Hansen, 2015: Solar forcing synchronizes decadal North Atlantic climate variability. *Nat. Commun.*, **6**, 8268, doi:10.1038/ncomms9268.

Tourpali, K., C. J. E. Schuurmans, R. van Dorland, B. Steil, and C. Brühl, 2003: Stratospheric and tropospheric response to enhanced solar UV radiation: A model study. *Geophys. Res. Lett.*, **30**, 1231, doi:10.1029/2002GL016650.

Tung, K. K., and R. S. Lindzen, 1979a: A theory of stationary long waves. Part I: A simple theory of blocking. *Mon. Wea. Rev.*, **107**, 714–734, doi:10.1175/1520-0493(1979)107<0714:ATOSLW>2.0.CO;2.

——, and ——, 1979b: A theory of stationary long waves. Part II: Resonant Rossby waves in the presence of realistic vertical shears. *Mon. Wea. Rev.*, **107**, 735–750, doi:10.1175/1520-0493(1979)107<0735:ATOSLW>2.0.CO;2.

Vallis, G. K., 2006: *Atmospheric and Oceanic Fluid Dynamics*. Cambridge University Press, 745 pp.

Viereck, R. A., and L. C. Puga, 1999: The NOAA Mg II core-to-wing solar index: Construction of a 20-year time series of chromospheric variability from multiple satellites. *J. Geophys. Res.*, **104**, 9995–10 005, doi:10.1029/1998JA900163.

Woollings, T., A. Hannachi, and B. Hoskins, 2010a: Variability of the North Atlantic eddy-driven jet stream. *Quart. J. Roy. Meteor. Soc.*, **136**, 856–868, doi:10.1002/qj.625.

——, M. Lockwood, G. Masato, C. Bell, and L. Gray, 2010b: Enhanced signature of solar variability in Eurasian winter climate. *Geophys. Res. Lett.*, **37**, L2805, doi:10.1029/2010GL044601.